applied sciences

MDPI

Article

Analysis of the Influence of Single-Walled Carbon Nanotubes on the Fluid–Structure Interaction Vibration Control in Bionic Hydraulic Pipelines

Lingxiao Quan [1,2], Jing Gao [1], Changhong Guo [1,*] and Jiacheng Yao [1]

[1] School of Mechanical Engineering, Yanshan University, Qinhuangdao 066004, China; lingxiao@ysu.edu.cn (L.Q.); 18233510132@163.com (J.G.)
[2] Hebei Provincial Key Laboratory of Heavy Machinery Fluid Power Transmission and Control, Yanshan University, Qinhuangdao 066004, China
* Correspondence: guochanghong@ysu.edu.cn

Abstract: In previous research, a bionic hydraulic pipeline (BHP) with a three-layer structure for absorbing pulsation was invented. This paper proposes to disperse single-walled carbon nanotubes (SWCNTs) in the elastic layer material, namely silicone rubber (RTV), to enhance its ability to absorb pulsation. Firstly, the RTV-SWCNTs composite specimens with different SWCNT proportions are prepared and tested. It was found that the mechanical property is optimal when the volume content of the SWCNTs is 0.5 vol%. On this basis, BHPs with RTV-SWCNTs composite material as the elastic layer are fabricated to study the influence of the thickness and length of the elastic layer on the absorption flow pulsation. The results show that the addition of SWCNTs significantly improves the mechanical properties of silicone rubber and reduces the friction between the elastic material and oil, so that the BHP can absorb the pressure pulsation better. With the appropriate thickness and length of the elastic layer, the addition of SWCNTs can increase the pulsation suppression effect by 20%. Moreover, to analyze the influence of nanomaterials on pipeline friction, a comprehensive fourteen-equation model for describing the fluid–structure interaction (FSI) of the pipe conveying fluid considering friction coupling is established. And through numerical analysis and modal tests, the evaluation error for the modified dynamic model of the BHP is less than 5%, verifying the correctness of the proposed model and solution method.

Keywords: carbon nanotubes; pulsation absorption; bidirectional fluid–structure interaction; friction coupling; bionic pipeline

Citation: Quan, L.; Gao, J.; Guo, C.; Yao, J. Analysis of the Influence of Single-Walled Carbon Nanotubes on the Fluid–Structure Interaction Vibration Control in Bionic Hydraulic Pipelines. *Appl. Sci.* **2023**, *13*, 8862. https://doi.org/10.3390/app13158862

Academic Editor: Loránd Szabó

Received: 12 July 2023
Revised: 27 July 2023
Accepted: 28 July 2023
Published: 1 August 2023

1. Introduction

The hydraulic pipeline is considered the "blood vessel" of mechanical equipment used for hydraulic transmission. Its function is to transmit power and energy. Meanwhile, the pipeline system with excellent mechanical properties and a reasonable structure can also absorb the pressure pulsation in the hydraulic system [1]. These functions are particularly important in aviation equipment. "High speed, high pressure and high power to weight ratio" is one of the main development directions in the aviation hydraulic system and mobile machines [2]. Meanwhile, it also entails greater requirements for the stability and reliability of the hydraulic pipeline system. Due to the high speed and high pressure, as well as the complex spatial structure of the pipeline, the vibration mechanism for the aviation hydraulic system is complex, making vibration control more difficult [3].

Many scholars have conducted a lot of research on the vibration control of hydraulic systems. According to the mechanism, vibration control in the hydraulic pipeline includes passive control and active control. Passive control is realized by installing dampers, vibration absorbers, attenuators, and sticking damping materials. Zang [4] studied the vibration absorption of a functionally graded materials fluid-conveying pipe coupled with

NiTiNOL–steel, and the effects of structure parameters on the absorption performance. The results show that NiTi–steel is an effective means of vibration absorption. Jiao [5] designed a magnetic interaction-based vibration absorber for continuous beams, which has a significant role in the vibration suppression of continuous structures. Chirathalattu [6] investigated the effectiveness of passive vibration suppression for an FSI system using a nonlinear energy sink. Shu [7] proposed a vibration control method for the typical pipelines used in armored vehicles by changing the pipe diameter, bending the radius, and increasing the pipeline branches, etc. Karimi [8] used a beam-based dynamic vibration absorber (beam DVA) to analyze pipes with different sizes of harmonic excitation at different frequencies, which showed that the mass ratio and stiffness ratio, respectively, have the highest and lowest impact on pipe vibration absorption. Based on the sensitivity analysis method and the Pareto optimal multi-objective genetic algorithm, Quan [9] optimized the parameters for the pipeline support and proposed an optimization method for the passive vibration control parameters in the aviation hydraulic pipeline. Although passive control has a clear damping mechanism, a simple structure, and easy implementation, its control frequency range is narrow, the effect of damping low-frequency vibration is limited, and the control parameters are not variable. Active control acquires vibration signals through sensing elements, obtains control signals through control algorithms, and applies them to actuators to achieve vibration control in the pipeline system. Guan [10] designed a piezoelectric direct drive spool valve that could adjust the parameters with the adaptive optimal control method to reduce the pressure pulsation amplitude to a low level. Cheer [11] studied a noninvasive structure controller composed of piezoelectric laminated actuators. And the experiment proved that the controller could achieve around 20 dB of attenuation in the dominantly radiating modes. Zhang [12,13] proposed an active constrained layer damping (ACLD) system with piezoelectric materials, with the aim of investigating the vibration and damping effect of an ACLD pipeline under fixed support. Active control technology has good characteristics for pipeline vibration and a good vibration suppression effect for low-frequency vibration, but its control algorithm is relatively complex, and the parallel structure makes the fluid flow state more complicated.

Given the existing problems with pipeline vibration control technology, researchers have begun to pay attention to the application of nanomaterials for vibration control in hydraulic pipelines. Arenas [14] studied a nanocomposite made of thermoplastic polyurethane (TPU) with laponite clay filler, which can improve the impact of sound insulation performance at a resonance frequency compared with TPU. Lubecki [15] studied the application of composite materials in hydraulic hoses and conducted experimental studies on dynamic changes in the length of a microhydraulic hose under the influence of step pressure and flow load. Rafie [16] studied the vibration and damping properties of epoxy composites modified with pristine and amino-functionalized graphene nanoplatelets (GNPs) at four different nanofiller loadings. Swain [17,18] conducted viscoelastic modeling and vibration analysis on nanocomposite shell panels with different CNTs and presented a detailed mathematical formulation for the determination of viscoelastic properties. Pan [19] prepared single-walled carbon nanotubes (SWCNTs)/7075 aluminum matrix composites to investigate the effects of different SWNTs contents on the microstructure and mechanical properties. The results show that with the increase in SWCNTs, the strength and hardness of the composites increase first and then decrease. Considering the excellent properties of nanomaterials in tribology and vibration reduction applications, in this paper, SWCNTs are uniformly dispersed in the matrix material (silicone rubber) by noncovalent modification. Thus, based on the previous research on double-layer bionic hydraulic pipelines (BHPs) [20], three-layer BHPs are made and the FSI analysis and experimental verification are conducted to study the influence of nanomaterials on the damping effect of BHPs, to further promote the research on BHPs in vibration reduction.

In this paper, RTV-SWCNTs composites with different SWCNT content are prepared, and the optimal mass ratio for their performance is obtained through experiments. Based on the constitutive equation for elastic material and the effect of friction coupling, the dynamic

model of BHP is established, and the model is validated through hammering modal experiments. Through the bidirectional FSI analysis in ANSYS and experimental research, the influence of the length and thickness of the elastic layer on the pulsation suppression effect is discussed and compared with the double-layer BHP. Finally, several key issues to be further studied in the future concerning bionic hydraulic pipelines are discussed.

2. Materials and Methods

2.1. The Structure of Three-Layer BHP

The structure of the three-layer BHP has been described in detail in [20], this is just a brief introduction here. The structure of the BHP is shown in Figure 1. The outer layer is made of stainless steel for support. The middle layer is the elastic layer, which plays a role in absorbing and weakening the flow pulsation. And the inner layer is composed of nanomaterials and an elastic matrix. SWCNTs are added to the matrix to form a smooth film on the surface of the elastic layer, which can reduce the flow resistance and stabilize the flow.

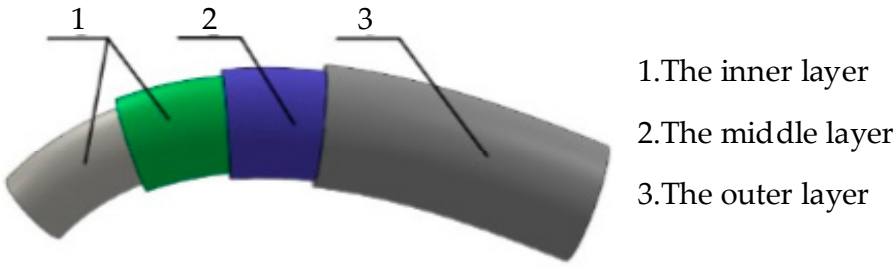

Figure 1. Structure schematic of the three-layer BHP structure.

2.2. The Preparation of RTV-SWCNTs Composite

To improve the mechanical properties of the polymer matrix, the surface modification of the SWCNTs is needed to improve its dispersion. The existing modification technologies can be roughly divided into two categories: covalent functionalization and noncovalent functionalization [21]. In this paper, noncovalent functionalization is used to modify the surface of the SWCNTs. Two-component room temperature vulcanized silicone rubber (RTV) is used as the matrix material, which consists of rubber (component A) and a cross-linking agent (component B). SWCNTs are used as the reinforced phase, and tetrahydrofuran (THF), which is a volatile solvent, is used as the dispersant. RTV-SWCNTs composites with SWCNT volume contents of 0.25 vol%, 0.5 vol%, 1 vol%, 2 vol%, and 4 vol% are prepared, respectively. Each SWCNTs-A solution is treated in a static state to observe whether there is precipitation in the solution and to preliminarily judge the dispersion of the SWCNTs in the RTV. The SWCNTs-A solution samples standing for 48 h are shown in Figure 2.

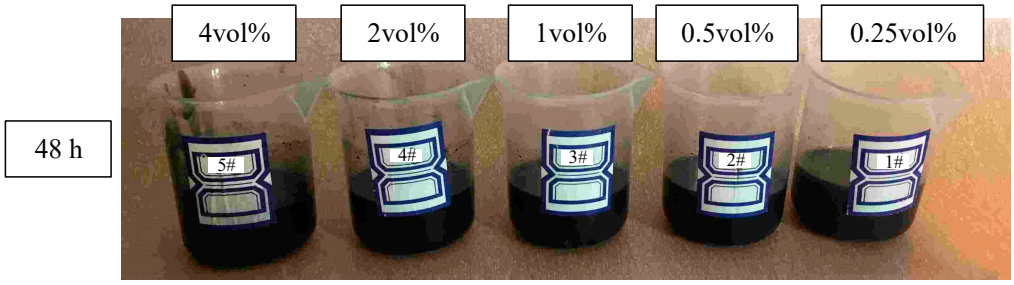

Figure 2. SWCNTs-A solution samples after 48 h of precipitation.

It could be seen that there was no precipitation of the SWCNTs in the SWCNTs-A solution, indicating that the solvent THF can disperse the SWCNTs in component A of the RTV.

2.3. Performance Test for RTV-SWCNTs Composite

Firstly, pour the prepared RTV-SWCNTs composite material solution into a dumbbell-shaped tensile mold, and cure at room temperature to prepare the tensile specimens. Then, the mechanical properties are tested using a tensile testing machine to obtain the performance parameters for the composite. Finally, the dispersion of the CNTs in the matrix material is observed through scanning electron microscope (SEM) experiments to find the RTV-SWCNTs composite material with the best performance.

2.3.1. RTV-SWCNTs Composite Tensile Test

The RTV-SWCNTs composites are subjected to tensile experiments to measure their elastic modulus, shear modulus, and Poisson's ratio. The tensile test machine used in this experiment is the Inspekt Table 100 tensile testing machine produced by Hegewald & Peschke, Germany, as shown in Figure 3. The tensile properties of the RTV-SWCNTs composites are tested at room temperature.

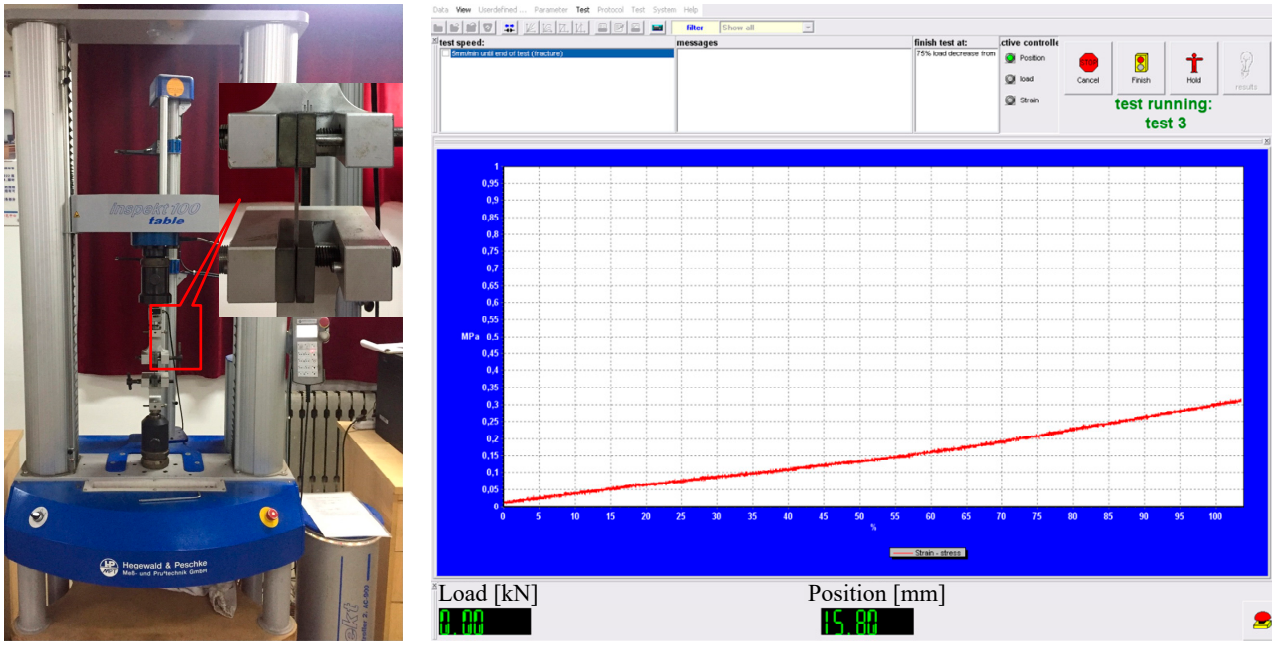

Figure 3. The tensile test bench and data acquisition program.

The mechanical properties of the RTV-SWCNTs composites with CNT contents of 0 vol%, 0.25 vol%, 0.5 vol%, 1 vol%, 2 vol%, and 4 vol% are tested. Three tensile specimens are prepared for each component group to reduce errors caused by measurement or other factors.

The stress–strain relationship of the RTV-SWCNTs composite material is non-linear. Because the elastic layer of the BHP has small deformation, the Mooney–Rivlin (M-R) constitutive model is used to describe the constitutive model of RTV-SWCNTs composites [20–25].

$$\sigma_\theta = 2C_{01}\left(3\varepsilon_\theta - 6\varepsilon_\theta^2\right) + 2C_{10}\left(3\varepsilon_\theta - 3\varepsilon_\theta^2\right) \quad (1)$$

where C_{10} and C_{01} are temperature-dependent material parameters. Then Equation (1) is simplified as:

$$\frac{\sigma_\theta}{6\left(\varepsilon_\theta - \varepsilon_\theta^2\right)} = C_{01}\left(1 - \frac{\varepsilon_\theta^2}{\varepsilon_\theta - \varepsilon_\theta^2}\right) + C_{10} \quad (2)$$

Among them, σ_θ is the stress of composite, and ε_θ is the strain of the composite. If, $x = 1 - \varepsilon_\theta^2\left(\varepsilon_\theta - \varepsilon_\theta^2\right)$, $y = \sigma_\theta / 6\left(\varepsilon_\theta - \varepsilon_\theta^2\right)$ Equation (2) can be abbreviated to,

$$y = C_{01}x + C_{10} \quad (3)$$

The tensile test data is substituted into Equation (2), and after linear fitting, the composite parameters C_{10} and C_{01} are obtained.

When the elastic material RTV is subject to small and medium deformation, the relationship between the elastic modulus E and the shear model G is as follows [26],

$$G = E/2(1+\mu) \tag{4}$$

Due to the incompressibility of RTV, Poisson's ratio μ = 0.5 can be substituted into Equation (4) to obtain $E = 3G$. Among them, the relationship between the shear modulus G and the parameters C_{10} and C_{01} is,

$$G = 2(C_{10} + C_{01}) \tag{5}$$

So, $E = 6(C_{10} + C_{01})$

2.3.2. Fracture Morphology Observation of Composite Materials

To better observe the fracture mechanism of the composites and the dispersion degree of the SWCNTs in the matrix material, SEM experiments are conducted on the specimens after tensile test fracture. The scanning electron microscope used in this experiment is the S-4800II cold field emission SEM by Hitachi, Japan. Table 1 shows the specific technical parameters for the SEM.

Table 1. Technical parameters of the scanning electron microscopy.

Name	Electron Beam Acceleration Voltage (kV)	Amplification (Times)	Resolution (nm)	Maximum Sample Size (mm)
value	0.5~30	30~800,000	1 (15 kV)	Φ100

3. Theoretical Modeling

3.1. Dynamic Model Considering Friction Coupling of the BHP

3.1.1. The FSI Dynamic Model

The force schematic diagram of the BHP is established according to the right-hand rule shown in Figure 4. To establish the dynamic model, we assume that the pipeline is installed parallel to the horizontal plane.

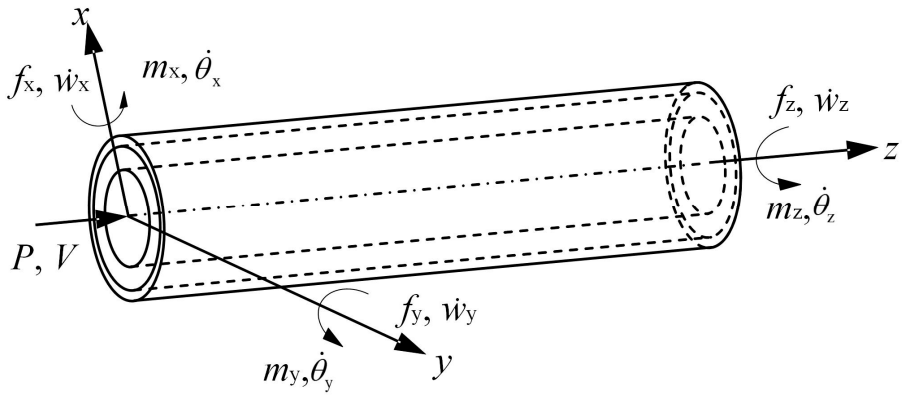

Figure 4. Force schematic diagram of the BHP.

Considering the influence of elastic material deformation, fluid viscous friction, pipeline, and fluid inertia [27], this paper establishes the FSI 14-equation for a single straight pipe as follows [20]:

Axial dynamic model:

$$\frac{1}{\rho_1}\frac{\partial P}{\partial z} + \frac{\partial V}{\partial t} + \frac{f_f}{A_1\rho_1} = 0 \tag{6}$$

$$\frac{\partial \dot{w}_z}{\partial t} + \frac{1}{\rho_t A_t + \rho_r A_r} \frac{\partial f_z}{\partial z} + \frac{f_f}{\rho_t A_t + \rho_r A_r} = 0 \tag{7}$$

$$\left[\frac{1}{K} + \frac{1}{3(C_{01} + C_{10})} \frac{r_r}{e_t + e_r}\right] \frac{\partial P}{\partial t} + \frac{\partial V}{\partial z} = 0 \tag{8}$$

$$\frac{\partial \dot{w}_z}{\partial z} + \frac{1 + v_r}{6C_{10} + 6C_{01}} \frac{1}{A_t + A_r} \frac{\partial f_z}{\partial t} + \frac{v_r}{6C_{10} + 6C_{01}} \frac{r_r}{e_t + e_r} \frac{\partial P}{\partial t} = 0 \tag{9}$$

X-*z* plane vibration equation for the BHP:

$$\frac{\partial f_x}{\partial z} + (\rho_t A_t + \rho_r A_r + \rho_1 A_1) \frac{\partial \dot{w}_x}{\partial t} + (\rho_t A_t + \rho_r A_r + \rho_1 A_1) g = 0 \tag{10}$$

$$\frac{\partial f_x}{\partial t} + k(A_t G_t + A_r G_r) \left(\frac{\partial \dot{w}_z}{\partial z} - \dot{\theta}_y\right) = 0 \tag{11}$$

$$\frac{\partial m_y}{\partial z} + f_x + (\rho_t I_t + \rho_r I_r + \rho_1 I_1) \frac{\partial \dot{\theta}_y}{\partial t} = 0 \tag{12}$$

$$\frac{\partial m_y}{\partial t} + (E_t I_t + E_r I_r) \frac{\partial \dot{\theta}_y}{\partial z} = 0 \tag{13}$$

Y-*z* plane vibration equation for the BHP:

$$\frac{\partial f_y}{\partial z} + (\rho_t A_t + \rho_r A_r + \rho_1 A_1) \frac{\partial \dot{w}_y}{\partial t} = 0 \tag{14}$$

$$\frac{\partial f_y}{\partial t} + k(A_t G_t + A_r G_r) \left(\frac{\partial \dot{w}_y}{\partial z} + \dot{\theta}_x\right) = 0 \tag{15}$$

$$\frac{\partial m_x}{\partial z} + f_y + (\rho_t I_t + \rho_r I_r + \rho_1 I_1) \frac{\partial \dot{\theta}_x}{\partial t} = 0 \tag{16}$$

$$\frac{\partial m_x}{\partial t} + (E_t I_t + E_r I_r) \frac{\partial \dot{\theta}_x}{\partial z} = 0 \tag{17}$$

Torsional vibration equation for the BHP:

$$(\rho_t J_t + \rho_r J_r) \frac{\partial \dot{\theta}_z}{\partial t} + \frac{\partial m_z}{\partial z} = 0 \tag{18}$$

$$(G_t J_t + G_r J_r) \frac{\partial \dot{\theta}_z}{\partial z} + \frac{\partial m_z}{\partial t} = 0 \tag{19}$$

where V is the liquid flow rate (m/s), K is the liquid elastic modulus (MPa), P is the liquid pressure (MPa), ρ is the density (kg/m^3), g is the acceleration of gravity (m/s^2), E is the elastic modulus (MPa), υ is the material Poisson's ratio, G is the shear modulus (MPa), k is the shear distribution coefficient, w is the straight-line displacement (m) of the BHP, A is the cross-sectional area of each layer (m^2), θ is the angle of rotation (rad) of the BHP, f is the cross-section force of the BHP (N), m is the bending moment of the BHP (N·m), J is the polar moment of inertia (kg/m^2), r is the pipeline radius (m), e is the wall thickness for each layer (m), and I is the moment of inertia (kg/m^2). The subscripts x, y, and z are the coordinate axis direction, t is the quantity related to the stainless steel material on the outer layer of the pipeline, r is the quantity related to the elastic material in the pipeline, l is the quantity related to the fluid, and C_{10} and C_{01} are temperature-related parameters for the elastic materials, which can be obtained through experimental tests.

3.1.2. Establishment and Analysis of Friction Term of BHP

In the FSI 14-equation for the BHP, Equations (6) and (7) are the incompressible viscous fluid flow continuity equation (N-S equation) [28], which includes the friction term for the BHP. The specific form is:

$$f_{\mathrm{f}}(t) = 2\pi r_{\mathrm{r}} \tau_0(t) \tag{20}$$

τ_0 is the shear friction force of the fluid on the inner wall of the pipeline. The Laplace transform of Equation (20) is:

$$F_{\mathrm{f}}(s) = 2\pi r_{\mathrm{r}} \widetilde{\tau}_0(s) \tag{21}$$

According to the Newton friction formula, Zielke [29] established the wall shear force τ_0 in Equation (20) and obtained the relationship between the instantaneous laminar flow wall shear force τ_0 and the instantaneous average velocity and the weighted historical velocity. The specific expression is as follows:

$$\tau_{\mathrm{z}}(t) = \frac{4\rho_1 v_1}{r_{\mathrm{r}}} V(t) + \frac{4\rho_1 v_1}{r_{\mathrm{r}}} \int_0^t \frac{\partial V}{\partial t}(u) W(t-u) \mathrm{d}u \tag{22}$$

where W is the weighting function of dimensionless time τ, $\tau = v_1 t / r_{\mathrm{r}}$. The expression of $W(\tau)$ is:

$$W(\tau) = \begin{cases} \sum\limits_{i=1}^{5} e^{-m_i \tau}, \tau \geq 0.02 \\ \sum\limits_{i=1}^{6} n_i e^{(i-2)/2}, \tau < 0.02 \end{cases} \tag{23}$$

where the values for the weighted coefficients m_i and n_i are shown in Tables 2 and 3.

Table 2. Weighting coefficient m_i.

m_1	m_2	m_3	m_4	m_5
−26.3744	−70.80493	−135	−218.9216	−322.5544

Table 3. Weighting coefficient n_i.

n_1	n_2	n_3	n_4	n_5	n_6
0.2821	−1.25	1.0579	0.9375	0.3967	0.3516

Based on the theory proposed by Zielke, Brunone proposed a friction model for the turbulent flow. He believes that the wall shear force is related to the average flow velocity V, instantaneous acceleration $\partial V / \partial t$, and convection acceleration $\partial V / \partial z$ [30]. This model is widely used in the calculation of wall shear force in a turbulent flow. The expression of wall shear force in the Brunone model is:

$$\tau_B = \frac{\rho_1 f V |V|}{8} + \frac{\rho_1 D}{4} \cdot k_3 \left(\frac{\partial V}{\partial t} - \alpha \frac{\partial V}{\partial z} \right) \tag{24}$$

Among them, f is the friction coefficient under turbulent flow; α is the wave velocity of the water hammer; K_3 is the Brunson friction coefficient; this numerical value generally is an empirical value, which is determined by test or trial calculation.

Based on the Brunone friction model, Vardy established a semi-empirical and semi-theoretical formula for K_3 by introducing the assumption of global acceleration [31]:

$$k_3 = \sqrt{7.41 / Re^{k4}} / 2 \tag{25}$$

$$k_4 = \log\left(14.3 / Re^{0.05}\right) \tag{26}$$

The weighted function model by Zielke does not depend on empirical parameters, thus, it is more consistent with experimental test results on laminar flow and low Reynolds number turbulence calculations. In this paper, the fluid state in the BHP is the laminar flow, so the Zielke friction model is used as the friction term in the FSI 14-equation.

3.2. Boundary Matrix Model

The two ends of the BHP are blocked with mass blocks of m0 and mL, and the excitation force F is applied along the z-direction of the pipeline at the initial end. The overall boundary constraint equation for the BHP is consistent with [20]. It will not be repeated here, only the concrete form for the boundary matrix at both ends of the BHP is given.

$$\mathbf{D}_0 = \begin{bmatrix} 1 & 0 & -1 & 0 & & & & & & & & & & \\ 0 & A_1 & K_{z0} & 1 & & & & & & & & & & \\ & & & & Z_{x0} & 1 & 0 & 0 & & & & & & \\ & & & & 0 & 0 & -Y_{y0} & 1 & & & & & & \\ & & & & & & & & Z_{y0} & 1 & 0 & 0 & & \\ & & & & & & & & 0 & 0 & -Y_{x0} & 1 & & \\ & & & & & & & & & & & & -T_{z0} & 1 \end{bmatrix} \tag{27}$$

$$\mathbf{D}_0 = \begin{bmatrix} 1 & 0 & -1 & 0 & & & & & & & & & & \\ 0 & A_1 & -K_{zL} & 1 & & & & & & & & & & \\ & & & & -Z_{xL} & 1 & 0 & 0 & & & & & & \\ & & & & 0 & 0 & Y_{yL} & 1 & & & & & & \\ & & & & & & & & Z_{yL} & 1 & 0 & 0 & & \\ & & & & & & & & 0 & 0 & Y_{xL} & 1 & & \\ & & & & & & & & & & & & T_{zL} & 1 \end{bmatrix} \tag{28}$$

3.3. Excitation of the BHP

In the hydraulic pipeline system, the pipeline excitation form can be divided into two categories: fluid excitation and solid excitation. In this paper, the modal analysis for the BHP is carried out by solid excitation. The function form is,

$$F(t) = F_r[1(t) - 1(t - T)] \tag{29}$$

The initial end excitation vector for the BHP can be obtained by the Laplace transform of Equation (29),

$$\mathbf{Q}_0 = \begin{bmatrix} 0 & -(F_r/s)\left(1 - e^{-sT}\right) & 0 & 0 & 0 & 0 & 0 \end{bmatrix}^T \tag{30}$$

No excitation is applied at the end of the BHP, so its excitation vector is:

$$\mathbf{Q}_L = \begin{bmatrix} 0 & 0 & 0 & 0 & 0 & 0 & 0 \end{bmatrix}^T \tag{31}$$

4. Analysis Example and Methods

4.1. Frequency-Domain Characteristic Analysis and Experimental Verification of the FSI Dynamic Model

4.1.1. Analysis of Frequency-Domain Characteristics of FSI Dynamic Model

The specific parameters for the BHP are shown in Table A1 (Appendix A). A mechanical impact excitation is applied to the initial end of the BHP, where the mean value of the impact force F_r is 15,000 N and the knocking time T is 2 ms. The boundary matrix, excitation vector, and pipeline structure parameters are substituted into the FSI 14-equation for the BHP for the modal solution. The result is shown in Figure 5.

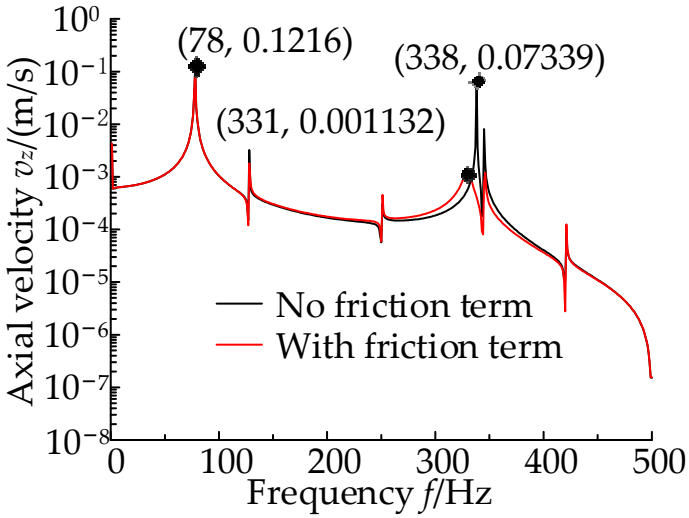

Figure 5. The curve on the effect of the friction term on the axial velocity of the BHP.

It can be observed that the frequency corresponding to each peak in the curve is the natural frequency of the BHP. By comparing the axial velocity response curve for the BHP with/without friction terms, it can be seen that friction coupling does not affect the resonant frequency, but affects its resonant peak.

4.1.2. Modal Verification Test

The modal experiment generally uses a hammer or the exciter as the excitation device. The experimental object in this paper is the BHP, which belongs to light and small equipment. The hammer is used as the excitation equipment and its specific technical parameters are shown in Figure 6a. Considering the effect of the oil on the pipeline, the oil is sealed in the pipeline. And the BHP filled with oil is suspended by a string with small rigidity. The acceleration sensor is stuck to the middle of the pipeline, as shown in Figure 6b. Then, the left end (inlet end) of the pipeline is knocked by the calibrated hammer to produce the frequency response curve.

Name	Parameter
Range	2000 N
Operating current	250 mA
Sensitivity	250 mA/N
Buffer head material	nylon
Hammer body mass	0.18 kg
Hammer head mass	0.006 kg

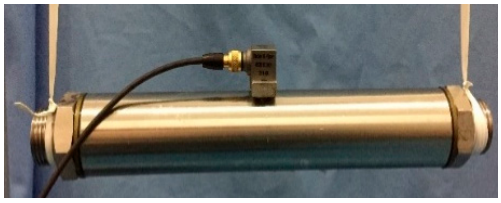

(**a**) (**b**)

Figure 6. Modal test. (**a**) Hammer used in the modal test. (**b**) The tested pipeline.

The modal experiment needs to collect the input signal and the output signal (acceleration signal). The collected input/output signals are transformed into the frequency domain using Fourier transform. Then, according to Equations (32)–(34), the auto-power spectrum of the input signal, the auto-power spectrum of the output signal, and the cross-power spectrum of the input–output signal are obtained, respectively. Finally, the frequency response curve for the axial velocity of the BHP is obtained by Equation (35), as shown in Figure 7.

$$G_{xx} = \frac{1}{N}\sum_{i=1}^{N} F_i^x F_i^{x^*} \tag{32}$$

$$G_{yy} = \frac{1}{N}\sum_{i=1}^{N} F_i^y F_i^{y^*} \tag{33}$$

$$G_{xy} = \frac{1}{N}\sum_{i=1}^{N} F_i^y F_i^{x^*} \tag{34}$$

$$H = \frac{G_{xy}}{G_{xx}} \tag{35}$$

where F is the data in the frequency domain after the Fourier transform, N is the number of sampling points, superscript $*$ represents the complex conjugate, subscript x is the input signal, and subscript y is the output signal.

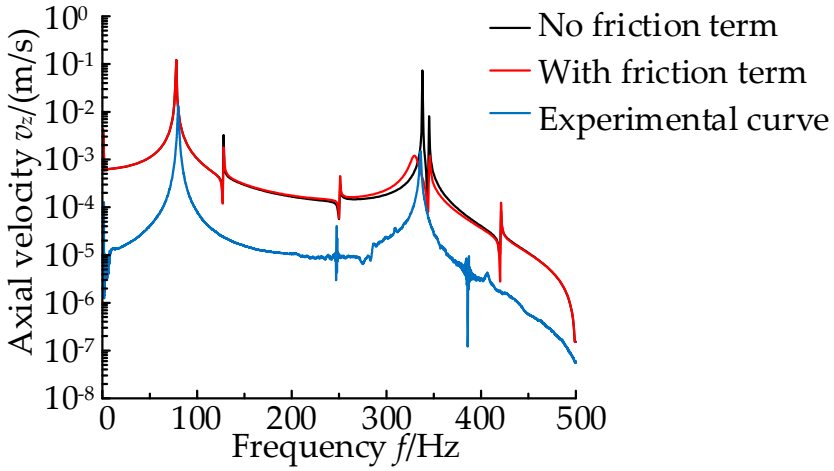

Figure 7. The frequency response curve for the BHP.

The comparison results for the experiment and simulation are shown in Table 4. The error between them is less than 5%. The validity of the FSI 14-equation dynamic model considering friction coupling is verified.

Table 4. Comparison of the modal analysis simulation and experimental data.

	Simulation (Hz)	Experimental (Hz)	Error (%)
First-order mode	78	81.26	4.01
Second-order mode	331	333.68	0.8

4.2. Bidirectional FSI Simulation and Experimental Methods for Bionic Pipelines

4.2.1. Simulation Analysis of Bidirectional FSI for the BHP

To study the influence of different types of BHP on the vibration of the pipe wall when the flow pulsation is the same, the bidirectional FSI analysis for the BHP is carried out in the ANSYS Workbench software. The grid division of the solid and fluid regions is shown in Figure 8. The structural parameters and fluid parameters are shown in Table A1; where, the parameters for the RTV are C_{01} = 1.213 MPa, C_{10} = −0.01679 MPa. The standard k-ξ, turbulence model is adopted for the fluid, the wall shear force in the BHP with RTV as the elastic layer is the wall shear force in the Brunone model, and the inner wall of the BHP with RTV-SWCNTs composite materials as the elastic layer is set as the smooth wall. The boundary condition for the pipeline inlet is set as the flow pulsation at the outlet of the axial piston pump, as shown in Figure 9. The pipeline outlet is set as the pressure outlet and the pressure is set as 2 MPa.

(**a**) (**b**)

Figure 8. Meshing in the BHP model. (**a**) Solid region sweep meshing method; (**b**) fluid region meshing method.

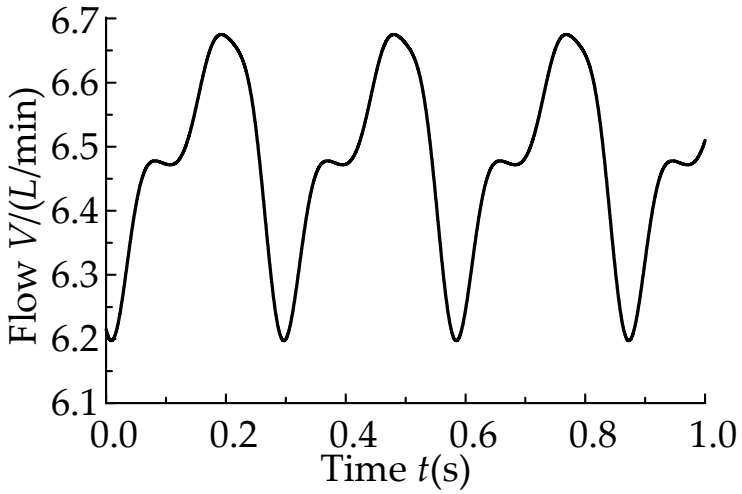

Figure 9. Flow pulsation curve for the bionic hydraulic pipeline inlet.

1. Influence of the thickness of the elastic layers on the vibration of the BHP

To study the effect of different thicknesses of the elastic layer and materials on the vibration of the pipeline wall in the BHP, the thickness of the stainless steel on the outer layer of the BHP is set at 2 mm, the length of the pipe is set at 100 mm, and the thickness of the elastic layer is, respectively, set at 5 mm, 10 mm, 20 mm, and 25 mm.

2. Influence of the length of the BHP on the vibration of the pipe wall

To study the effect of the different lengths and materials in the elastic layer on the vibration of the pipeline wall in the BHP, the thickness of the stainless steel on the outer layer of the BHP is set at 2 mm, the thickness of the elastic layer is set at 5 mm, and the length of the pipeline is, respectively, set at 100 mm, 150 mm, 250 mm, and 300 mm.

4.2.2. BHP Fabrication and Experimental System

The outer layer of the BHP is made of stainless steel and the middle layer is the elastic layer, which is composed of RTV-SWCNTs composite materials. The content of the SWCNTs in the RTV-SWCNTs composite materials is 0.5 vol%. Some of the SWCNTs adhered to the inner wall of the pipeline form a smooth film, forming the inner layer of the BHP. The double-layer BHP is used for a comparative experiment, whose outer layer is made of stainless steel and the inner layer is made of RTV. The BHP is shown in Figure 10. The structural parameters for the BHP specimens are shown in Table 5.

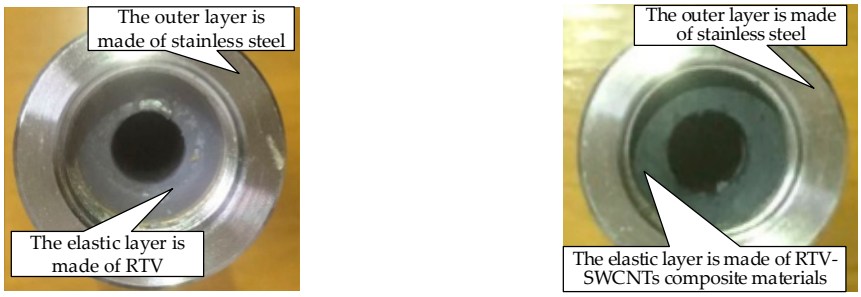

(**a**) (**b**)

Figure 10. Bionic hydraulic pipeline physical diagram. (**a**) BHP with RTV as the elastic layer; (**b**) BHP with RTV-SWCNTs composite materials as the elastic layer.

Table 5. The structural parameters for the BHP specimens.

No.	Length (mm)	Thickness of Elastic Layer (mm)	Thickness of Outer Layer (mm)	Inside Diameter (mm)
1	130	5	3	10
2	130	10	3	10
3	130	15	3	10
4	130	20	3	10
5	130	25	3	10
6	180	5	3	10
7	230	5	3	10
8	280	5	3	10
9	330	5	3	10

The experiment on the flow pulsation absorption of the BHP is to study the absorption effect of the length, the material in the elastic layer, and the thickness of the elastic layer in the BHP on the flow pulsation at the outlet of the axial piston pump, by comparing the outlet flow pulsation of the different types of BHP. The vibration experimental apparatus is shown in Figure A1 (Appendix B).

4.2.3. Experiment on the Vibration Absorption of the BHP

1. Influence of the thickness of the elastic layers on the flow pulsation

The No. 1–5 pipelines in Table 5 are installed at the outlet of the hydraulic pump, according to Figure A1. The pressure of the pipelines is set at 2 MPa.

2. Influence of the length of the BHP on the flow pulsation

The No.1, 6–9 pipelines in Table 5 are installed at the outlet of the pump, according to Figure A1. The flow pulsation curves for the different BHPs are shown in Figure 9.

3. Influence of the thickness of the elastic layers on the vibration of the BHP

The No. 1–5 pipes in Table 5 are installed at the outlet of the hydraulic pump, as shown in Figure A1. The load pressure of the pipeline is set to 2 MPa and the radial acceleration amplitude of the pipe wall at the middle node (point P) for each BHP is measured.

4. Influence of the length of the pipeline on the vibration of the BHP

The No. 1, 6–9 pipes in Table 5 are installed at the outlet of the hydraulic pump, as shown in Figure A1. The load pressure of the pipeline is set to 2 MPa and the radial acceleration amplitude of the pipe wall at point P for each BHP is measured.

5. Results and Discussion

5.1. Experimental Results on the Properties of the RTV-SWCNTs Composites

5.1.1. Tensile Test Results for the RTV-SWCNTs Composites

The tensile test results are shown in Figure 11.

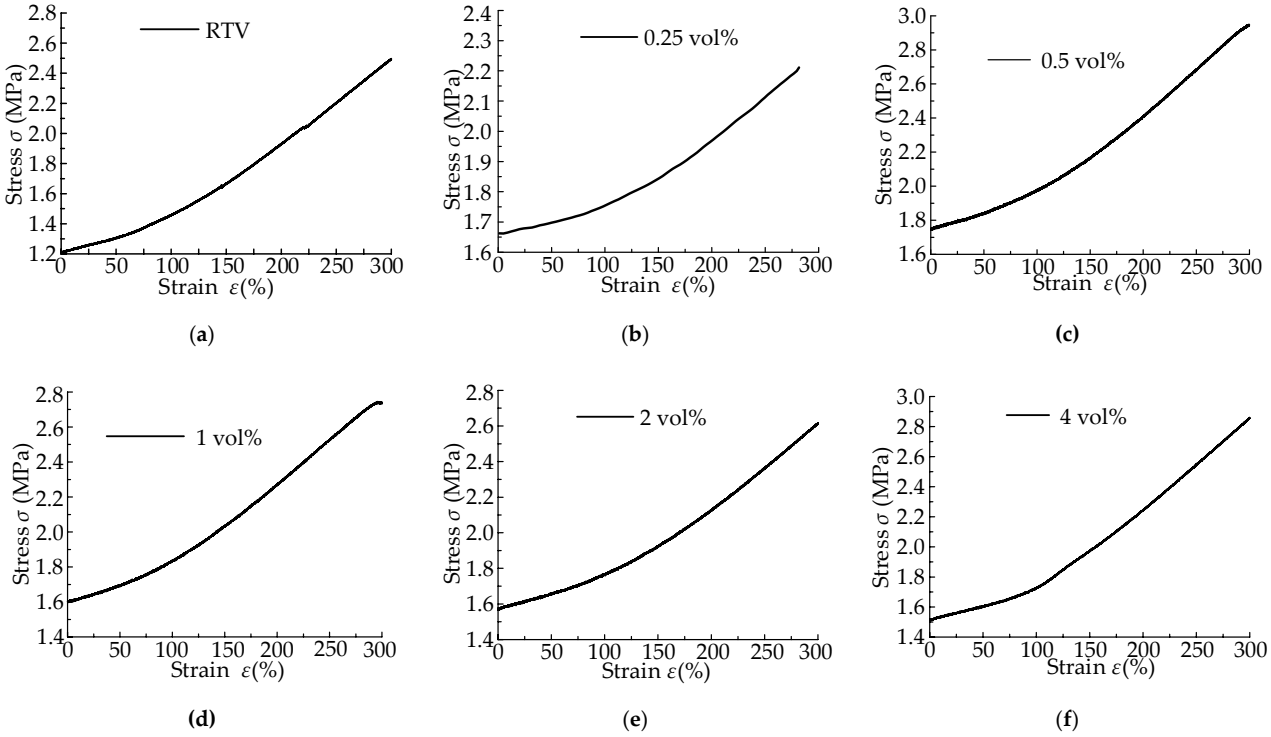

Figure 11. Stress–strain curve for the RTV-SWCNTs composites with different SWCNTs content. The content of the SWCNTs is: (**a**) 0 vol%; (**b**) 0.25 vol%; (**c**) 0.5 vol%; (**d**) 1 vol%; (**e**) 2 vol%; (**f**) 4 vol%.

Figure 12 shows the fitting curves for the composite materials under different SWC NT contents.

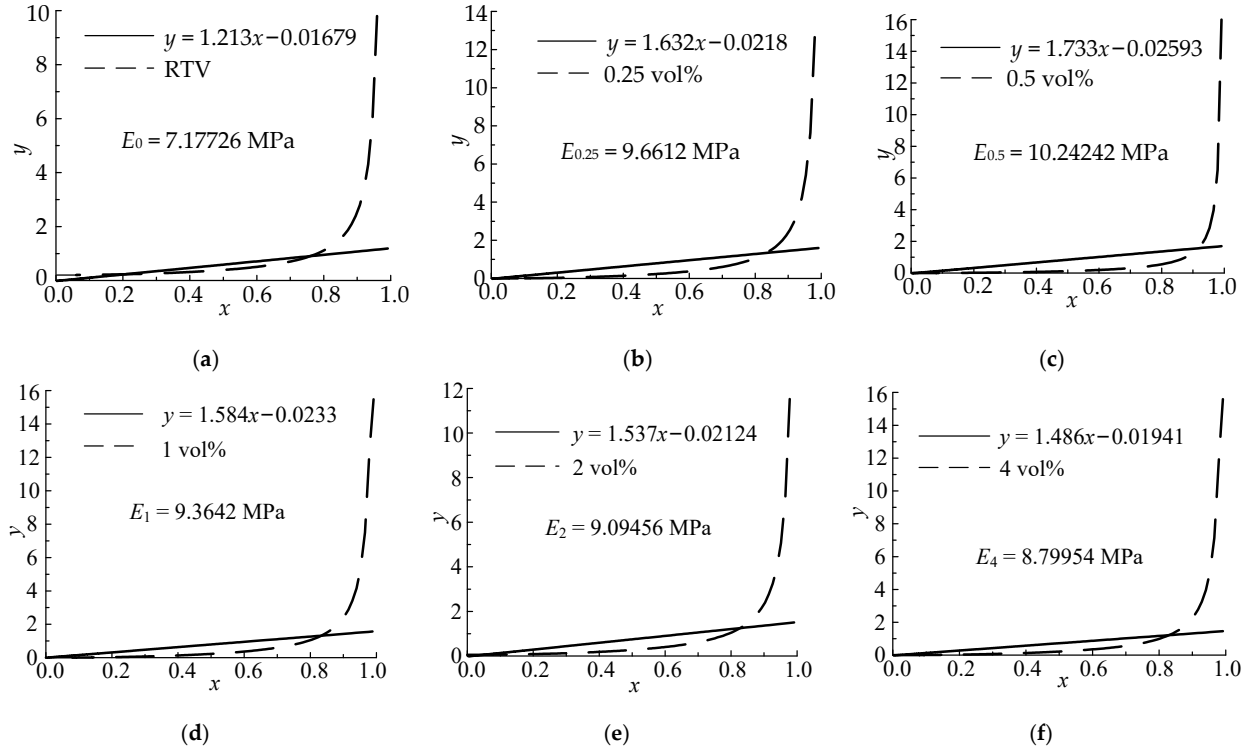

Figure 12. The fitting curve for the tensile experimental data on the composites with different SWCNTs content. The content of the SWCNTs is: (**a**) 0 vol%; (**b**) 0.25 vol%; (**c**) 0.5 vol%; (**d**) 1 vol%; (**e**) 2 vol%; (**f**) 4 vol%.

It can be seen that with the increase in the content of the SWCNTs, the elastic modulus first increases and then decreases. When the content of the SWCNTs is 0.5 vol%, the elastic modulus of the composite material reaches the maximum, which is 10.24242 MPa. And C_{10} = 1.733 MPa, C_{01} = −0.02593 MPa.

5.1.2. The Results of SEM Experiment on the Composite Materials

Under different SWCNT contents, the fracture morphology for each specimen is shown in Figure 13.

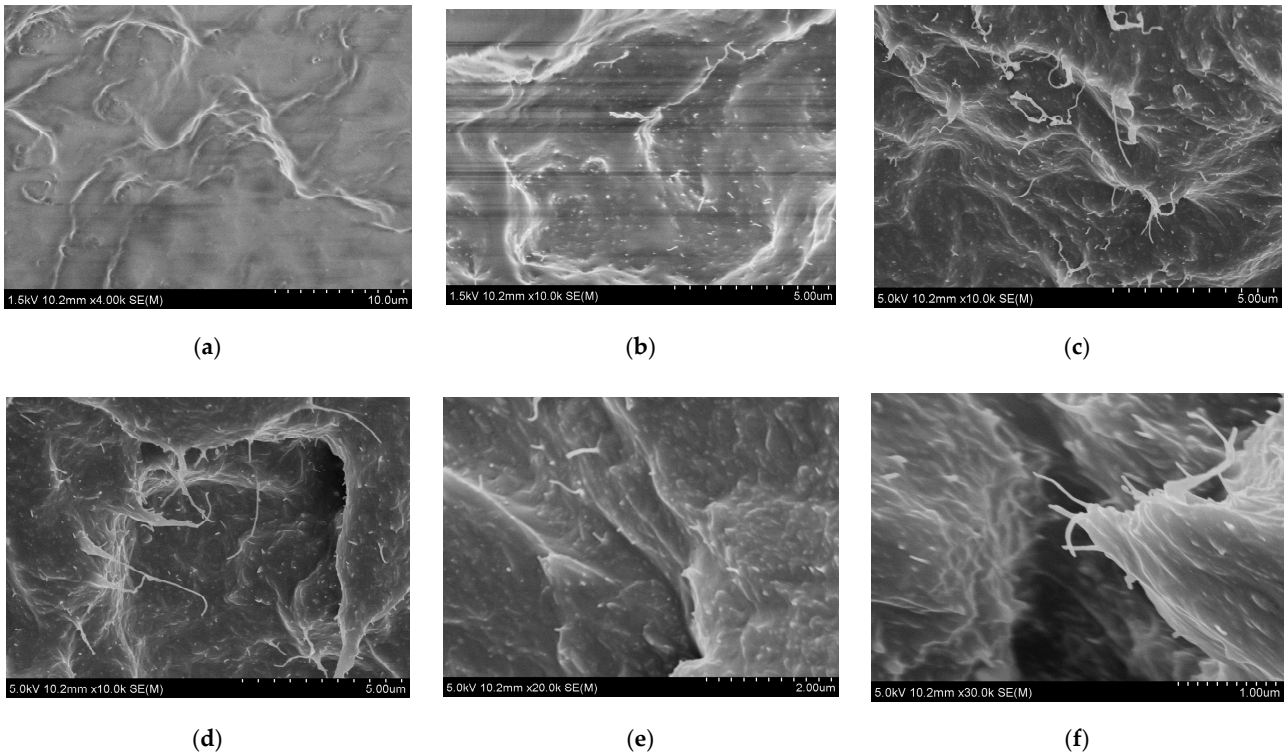

(**a**) (**b**) (**c**)

(**d**) (**e**) (**f**)

Figure 13. The fracture morphology for the specimens with different SWCNTs content under SEM. The content of the SWCNTs is: (**a**) 0 vol%; (**b**) 0.25 vol%; (**c**) 0.5 vol%; (**d**) 1 vol%; (**e**) 2 vol%; (**f**) 4 vol%.

In Figure 13a–c, when no SWCNTs are added to the matrix material, the fracture morphology is relatively smooth and has distinct folds, which is an obvious feature of a brittle fracture in the elastic material. As the content of the SWCNTs increases, the fracture morphology of the material gradually becomes rough and wrinkled, so the energy required in the stretching process increases, indicating that the tensile strength and elastic modulus of the material increase accordingly [32,33]. The surface roughness of the material in Figure 13d is similar to that in Figure 13c, but there are obvious pits on the surface. The pits are caused by the agglomeration of the SWCNTs, which indicates that the filling capacity of the SWCNTs has reached the supersaturated state. In Figure 13e,f, the pit phenomenon is more obvious, and the agglomeration is intensified, which indicates that the probability of CNTs agglomeration intensifies with the increase in the content.

Combined with the existing tensile experimental and SEM test data (the additional amount of the SWCNT is 0–4 vol%), when the content of the SWCNTs is 0.5 vol%, the mechanical properties of the RTV-SWCNTs composites are the best. Therefore, the RTV-SWCNTs composite material with the SWCNTs content of 0.5 vol% is used as the elastic layer material in the BHP.

5.2. Results from the BHP Bidirectional FSI Simulation

5.2.1. Simulation Results for the BHP Vibration with Different Elastic Layer Thicknesses

The curve for the radial acceleration at the middle node (point P) in the BHP with different thicknesses of the elastic layer is shown in Figure 14.

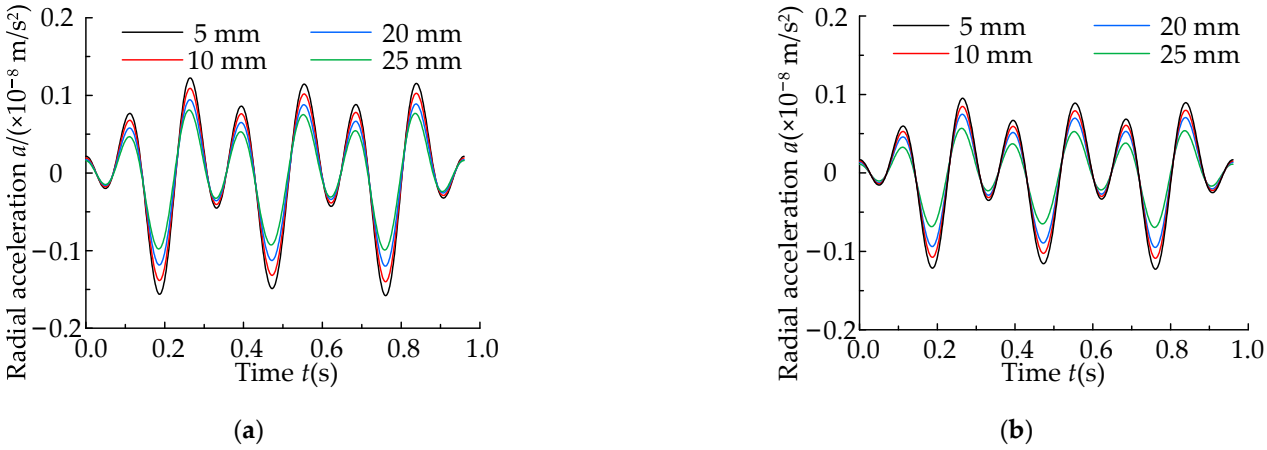

Figure 14. Radial acceleration at point P with different thicknesses of the elastic layer. (**a**) BHP with RTV as the elastic layer; (**b**) BHP with RTV-SWCNTs composite materials as the elastic layer.

As can be seen in Figure 14 that the amplitude of the radial acceleration in the BHP decreases with the increase in the thickness of the elastic layer.

Figure 15 shows the comparison curves for the radial acceleration at point P in the BHPs with RTV or SWCNTs added when the thickness of the elastic layer is the same.

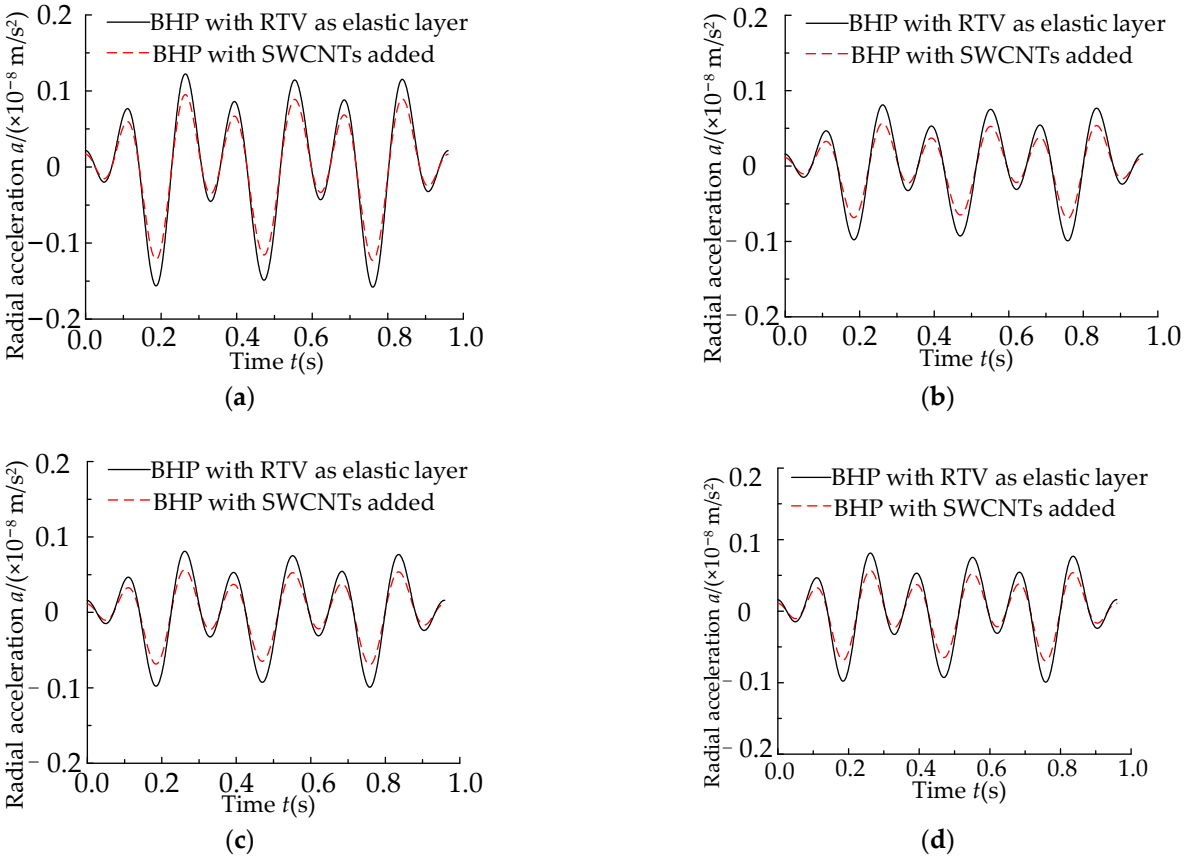

Figure 15. Radial acceleration at point P with different materials. The thickness of the elastic layer is (**a**) 5 mm; (**b**) 10 mm; (**c**) 20 mm; (**d**) 25 mm.

Figure 15 shows that when the thickness of the elastic layer is the same, the vibration acceleration in the three-layer BHP with SWCNTs added is lower than that of the double-layer BHP and the vibration absorption effect is better. Adding the SWCNTs to the elastic layer increases its tensile strength and the smooth inner wall of the pipeline can not only reduce the fluid resistance but also stabilize the flow.

The vibration reduction is 'the standard deviation of the radial acceleration of the BHP with RTV as the elastic layer minus the standard deviation of the radial acceleration of the BHP with RTV-SWCNTs composite material as the elastic layer'. The vibration reduction reflects the degree of vibration suppression in the BHP with the same elastic layer thickness and different materials, as shown in Table 6.

Table 6. The suppressive effect of the different thicknesses of the elastic layer on pipeline vibration.

Thickness (mm)	RTV	RTV-SWCNTs Composite Materials	Vibration Reduction (%)
	The Standard Deviation for the Vibration Acceleration		
5	7.58×10^{-10}	5.89×10^{-10}	22.3
10	6.73×10^{-10}	5.23×10^{-10}	22.3
20	5.775×10^{-10}	4.297×10^{-10}	25.6
25	4.82×10^{-10}	3.375×10^{-10}	29.98

It can be seen from Table 6 that the standard deviation for the radial acceleration in the three-layer BHP with SWCNTs added is significantly lower than that of the double-layer BHP with RTV as the elastic layer. And with the increase in the pipeline thickness, the suppressive effect of the vibration increases.

5.2.2. Simulation Results for BHP Vibration with Different Lengths of Pipeline

The curves for the radial acceleration at point P in the BHP with different lengths of the elastic layer are shown in Figure 16.

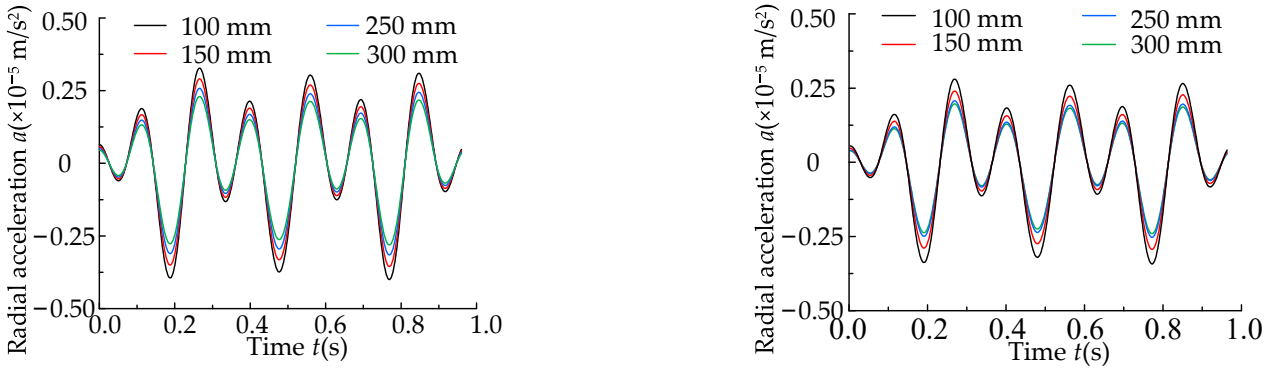

Figure 16. Radial acceleration at point P with different lengths of the elastic layer. (**a**) BHP with RTV as the elastic layer; (**b**) BHP with RTV-SWCNTs composite materials as the elastic layer.

In Figure 16, the amplitude of the radial acceleration in the BHP decreases with the increase in the pipeline length. In reference to Section 5.2.1, Figure A2 (in Appendix C) shows the radial acceleration curves for the BHPs with different elastic layer materials at P point when the pipe length is the same.

As shown in Figure A2, when the pipeline length is the same, the vibration acceleration in the three-layer BHP with SWCNTs added is lower than that of the double-layer BHP with RTV as the elastic layer, and the effect of the vibration absorption is better. The suppressive effect of the different lengths in the BHP on the vibration of the pipeline wall is shown in Table 7.

Table 7. The suppressive effect of the different lengths in the BHP on the vibration of the pipeline wall.

Length (mm)	RTV	RTV-SWCNTs Composite Materials	Vibration Reduction (%)
	The Standard Deviation for the Vibration Acceleration		
100	1.956×10^{-6}	1.675×10^{-6}	14.4
150	1.736×10^{-6}	1.435×10^{-6}	17.3
250	1.542×10^{-6}	1.237×10^{-6}	19.8
300	1.373×10^{-6}	1.176×10^{-6}	14.3

It can be seen that the standard deviation for the radial acceleration in the BHP with RTV-SWCNTs composite materials as the elastic layer is significantly lower than that of the BHP with RTV. And with the increase in the pipeline length, the suppressive effect of the vibration increases. Besides, when the length of the pipeline is 250 mm, the percentage of pulsation reduction in the pipeline is the largest and the effect of the vibration reduction is the best, which lays the foundation for further optimization in the design of the BHP.

5.3. Results from the BHP Vibration Experiment

5.3.1. Pulsation Absorption Experiment Results for the BHP with Different Thicknesses of Elastic Layer

The outlet flow pulsation curves for the different BHPs are shown in Figure 17.

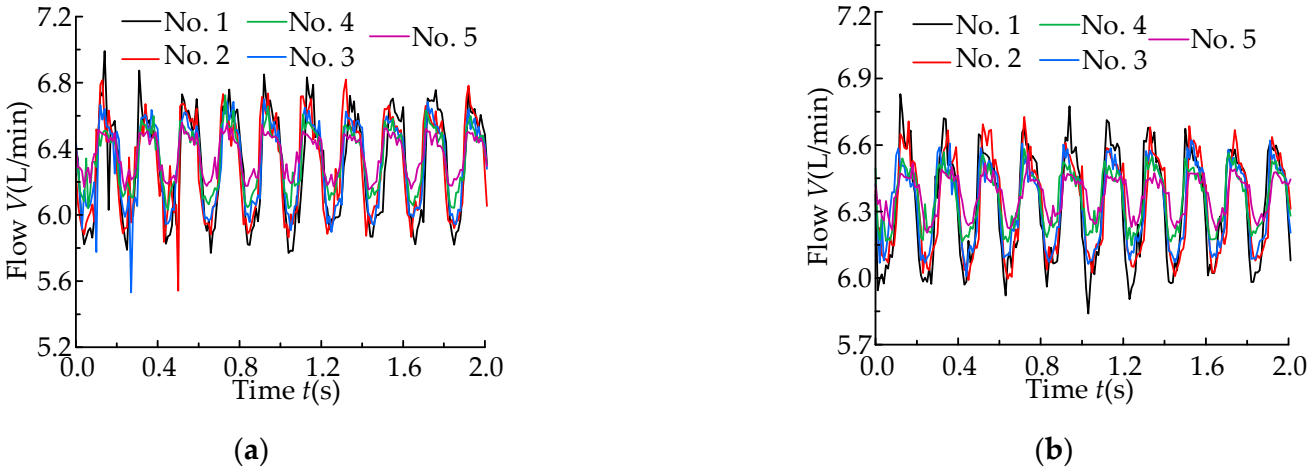

Figure 17. Effect of thickness of the elastic layer on flow pulsation. (**a**) BHP with RTV as the elastic layer; (**b**) BHP with RTV-SWCNTs composite materials as the elastic layer.

The amplitude of the flow pulsation at the outlet of the double-layer BHP with RTV as the elastic layer and the three-layer BHP with RTV-SWCNTs composite materials as the elastic layer decreases with the increase in the thickness of the elastic layer. This shows that the elastic materials (RTV and RTV-SWCNTs composite materials) have an absorption effect on the flow pulsation at the outlet of the hydraulic pump. And with the increase in the thickness of the pipeline, the absorption effect of the flow pulsation increases.

The comparison curves for the flow pulsation at the outlet of the double-layer BHP with RTV as the elastic layer and the three-layer BHP with RTV-SWCNTs composite materials as the elastic layer under the same thickness of the elastic layer are shown in Figure 18.

Figure 18 shows that the amplitude of the flow pulsation in the three-layer BHP with RTV-SWCNTs composite materials as the elastic layer is significantly lower than that of the double-layer BHP with RTV as the elastic layer.

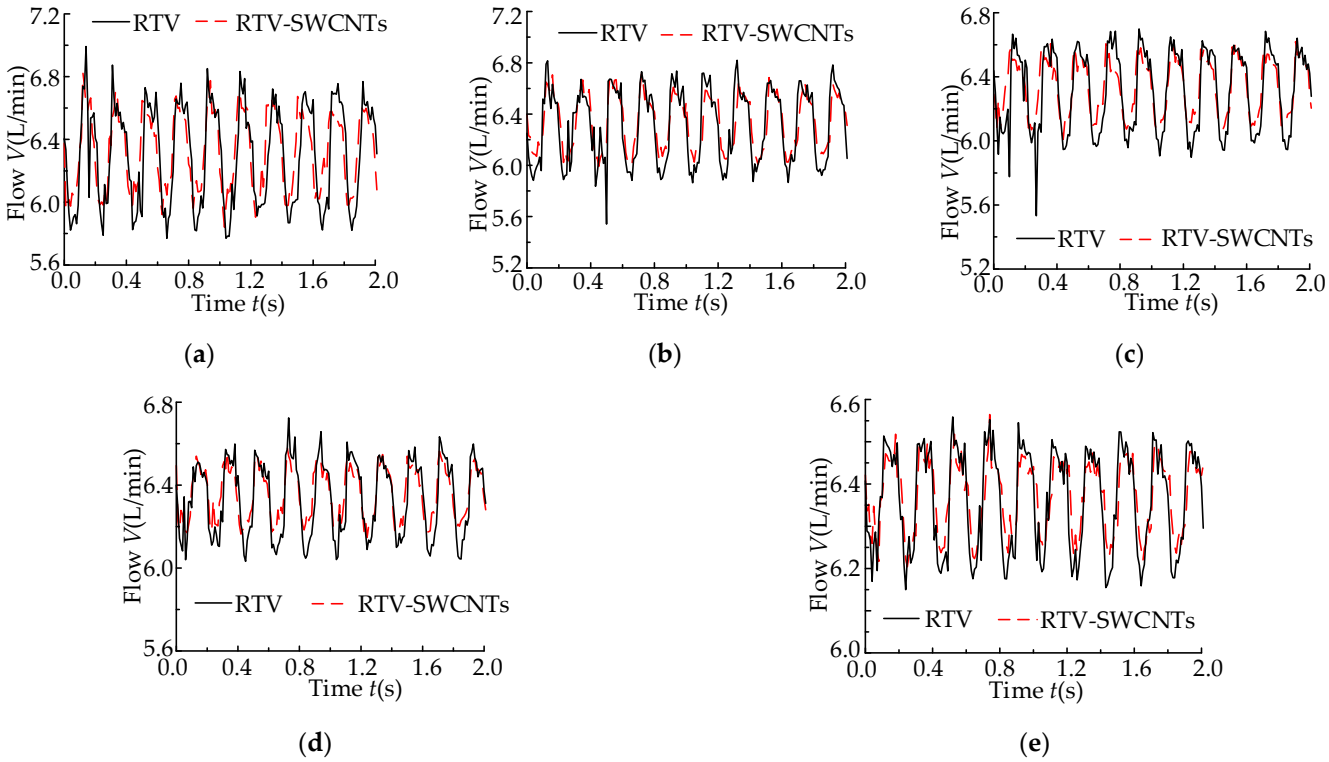

Figure 18. Effect of different elastic layer materials with the same thickness on flow pulsation. The thickness of the elastic layer is: (**a**) 5 mm; (**b**) 10 mm; (**c**) 15 mm; (**d**) 20 mm; (**e**) 25 mm.

The absorption effect of the flow pulsation in the BHPs with different thicknesses of the elastic layer is shown in Table 8. The pulsation reduction is 'the standard deviation of flow pulsation at the outlet of BHP with RTV as the elastic layer subtracts the standard deviation of flow pulsation at the outlet of BHP with RTV-SWCNTs as the composite elastic layer'. The pulsation reduction reflects the flow pulsation absorption effect for the BHP with the same pipeline thickness and different elastic layer materials.

Table 8. The absorption effect of the flow pulsation for the BHP with different thicknesses of the elastic layer.

No.	Thickness (mm)	RTV	RTV-SWCNTs Composite Materials	Pulsation Reduction (%)
		The Standard Deviation for the Flow Pulsation		
1	5	0.319	0.248	22.3
2	10	0.291	0.215	26.1
3	15	0.253	0.177	30.04
4	20	0.1802	0.128	28.97
5	25	0.1197	0.0872	27.15

The standard deviation for the flow pulsation in the three-layer BHP with SWCNTs added is significantly lower than that of the double-layer BHP with RTV as the elastic layer. With the increase in the thickness of the pipeline, the standard deviation for the flow pulsation at the outlet of the pipeline decreases, and the effect of the pulsation absorption increases. When the thickness of the elastic layer is 15 mm, the percentage of pulsation reduction is the largest and the absorption effect of the flow pulsation is the best, which lays the experimental foundation for further optimization of BHPs.

5.3.2. Pulsation Absorption Experiment Results for the BHP with Different Lengths of Pipeline

The flow pulsation curves for the different BHPs are shown in Figure 19. The amplitude of the flow pulsation at the outlet of both the double-layer BHP with RTV as the elastic layer and the three-layer BHP with RTV-SWCNTs composite materials as the elastic layer decreases with the increase in the length of the pipeline. In the limited length range of the experiment, the capacity of the BHP to absorb flow pulsation increases with the increase in its length.

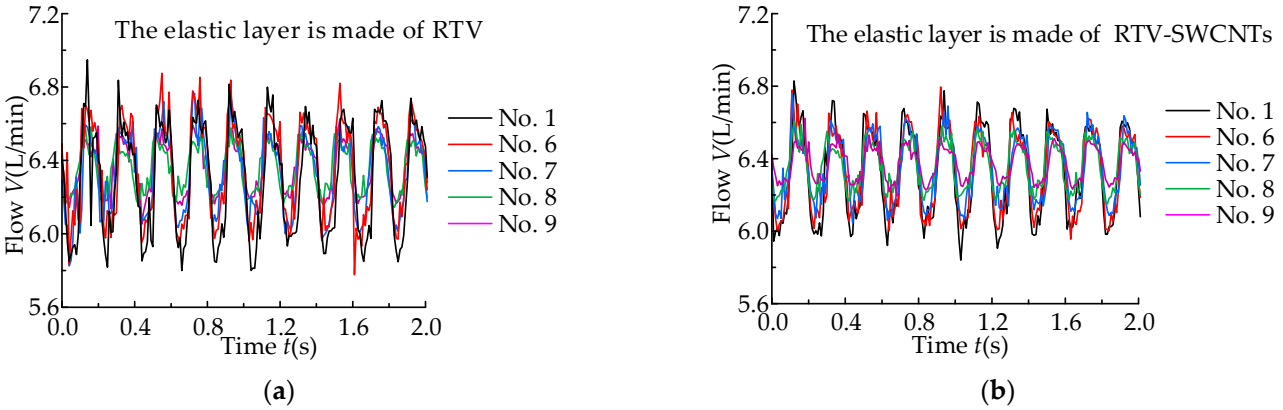

Figure 19. Flow pulsation curve for the BHP outlet. (**a**) RTV as the elastic layer; (**b**) RTV-SWCNTs composite as the elastic layer.

In reference to Section 5.3.1, the comparison curves for the flow pulsation at the outlet of the double-layer BHP with RTV or RTV-SWCNTs composite materials as the elastic layer under the same length of pipeline are shown in Figure A3 (Appendix C).

It can be seen from Figure A3 that the amplitude of the flow pulsation in the three-layer BHP with RTV-SWCNTs composite materials as the elastic layer is significantly lower than that of the double-layer BHP with RTV as the elastic layer. The absorption effect of the flow pulsation in the BHPs with different lengths is shown in Table 9.

Table 9. The absorption effect of flow pulsation in the BHPs with different lengths of pipeline.

No.	Length (mm)	RTV	RTV-SWCNTs Composite Materials	Pulsation Reduction (%)
		The Standard Deviation for Flow Pulsation		
1	130	0.319	0.248	22.3
6	180	0.301	0.216	28.2
7	230	0.2702	0.1779	34.16
8	280	0.1824	0.1296	28.9
9	330	0.128	0.0913	28.7

The standard deviation for the flow pulsation in the three-layer BHP with SWCNTs added is significantly lower than that of the double-layer BHP with RTV as the elastic layer. With the increase in the length of the pipeline, the standard deviation for the flow pulsation at the outlet of the pipeline decreases, and the effect of the pulsation absorption increases. When the length of the pipeline is 230 mm, the percentage of pulsation reduction is the largest and the absorption effect of the flow pulsation is the best, which lays the experimental foundation for further optimization of BHPs.

5.3.3. Vibration Experiment Results for the BHP with Different Elastic Layer Thicknesses

The radial acceleration amplitude for the pipe wall at the middle node (point P) in each BHP is shown in Figure 20.

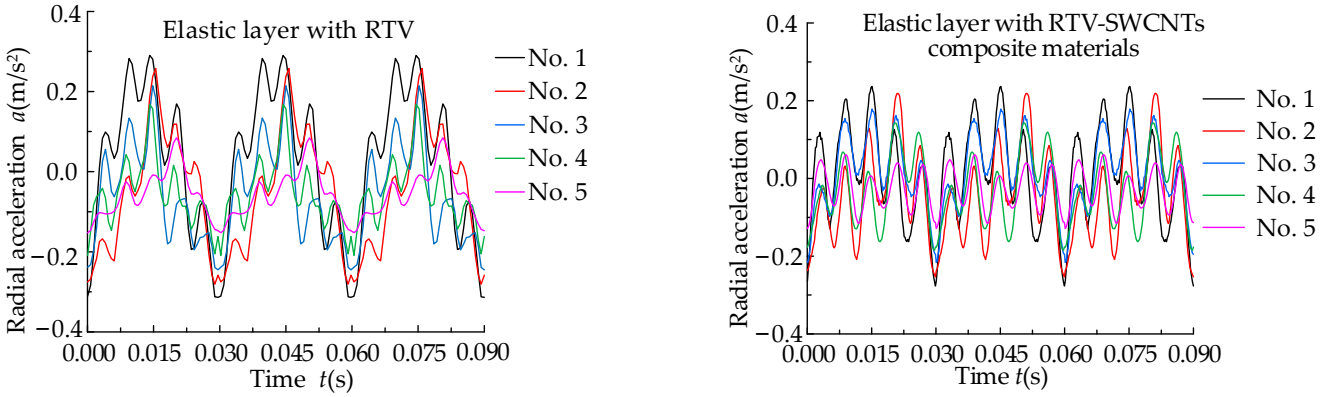

(**a**) (**b**)

Figure 20. Effect of elastic layer thickness on the radial acceleration at point P.(**a**) BHP with RTV as the elastic layer; (**b**) BHP with RTV-SWCNTs composite materials as the elastic layer.

The radial acceleration amplitude at point P in the two-layer BHP with RTV as the elastic layer and the three-layer BHP with RTV-SWCNTs composite as the elastic layer decreases as the thickness of the elastic layer increases. This indicates that elastic materials (RTV or RTV-SWCNTs composites) can suppress pipeline vibration by absorbing the flow pulsation. With the increase in the elastic layer thickness, the effect of the vibration suppression is more obvious.

In reference to Section 5.2.1, Figure A4 (Appendix C) compares the amplitude of the radial acceleration at point P in the BHPs with RTV or RTV-SWCNTs composite as the elastic layer when the thickness of the elastic layer is the same.

In Figure A4, it can be seen that the radial acceleration at point P in the three-layer BHP with RTV-SWCNTs composite material as the elastic layer is significantly lower than that of double-layer BHP with RTV as the elastic layer. The data on the vibration suppression effect in the BHP with different thicknesses of the elastic layer is shown in Table 10.

Table 10. Suppression effect in BHPs with different thicknesses of the elastic layer on pipe vibration.

No.	Thickness (mm)	RTV	RTV-SWCNTs Composite Materials	Vibration Reduction(%)
		The Standard Deviation for Radial Acceleration		
1	5	0.179	0.162	9.5
2	10	0.143	0.106	25.9
3	15	0.1202	0.0758	36.9
4	20	0.098	0.0689	29.7
5	25	0.0892	0.0689	22.8

It can be seen that the standard deviation for the radial acceleration in the three-layer BHP with SWCNTs is significantly lower than that of double-layer BHP with RTV as the elastic layer. As the thickness increases, the standard deviation for the radial acceleration decreases, and the effect of the pulsation absorption increases. When the thickness of the elastic layer is 15 mm, the percentage of the pulsation reduction is the largest, and the vibration suppression effect in the BHP is the best. This conclusion lays the experimental foundation for the further optimization of BHPs.

5.3.4. Vibration Experiment Results for the BHP with Different Lengths of Pipeline

The radial acceleration amplitude for the pipe wall at point P for each BHP is shown in Figure 21.

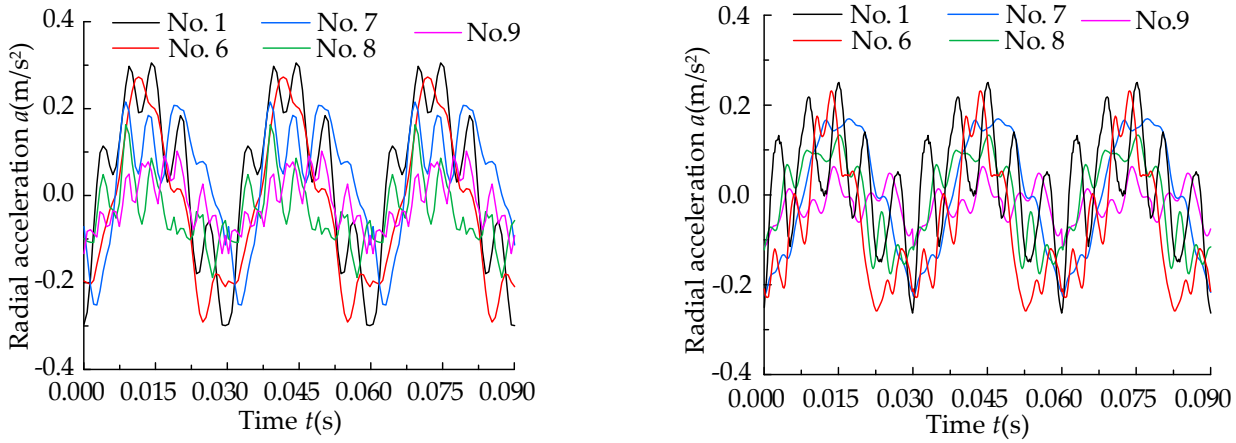

Figure 21. Effect of the length of the elastic layer on the radial acceleration at point P. (**a**) RTV as the elastic layer; (**b**) RTV-SWCNTs composite materials as the elastic layer.

The radial acceleration amplitude in the double-layer BHP with RTV as the elastic layer and the three-layer BHP with RTV-SWCNTs composite material as the elastic layer both decreased with the increase in the pipeline length. Moreover, as the length increases, the vibration suppression effect in the BHP on the pipeline system increases.

In reference to Section 5.2.1, Figure A5 (in Appendix C) compares the radial acceleration amplitude in the BHP with the same pipeline length and different elastic layers.

As shown in Figure A5, the acceleration amplitude in the three-layer BHP with RTV-SWCNTs composite as the elastic layer is significantly lower than that of the double-layer BHP with RTV as the elastic layer.

The vibration suppression effect of the BHPs with different lengths of pipeline is shown in Table 11.

Table 11. Suppression effect in the BHPs with different lengths of pipeline on pipe vibration.

No.	Length (mm)	RTV	RTV-SWCNTs Composite Materials	Vibration Reduction (%)
		The Standard Deviation for Radial Acceleration		
1	130	0.179	0.174	2.8
6	180	0.138	0.132	4.3
7	230	0.1202	0.102	15.14
8	280	0.108	0.0615	43.1
9	330	0.0712	0.03697	48.1

The standard deviation for the radial acceleration in the three-layer BHP with SWCNTs added is significantly lower than that of the double-layer BHP with RTV as the elastic layer. As the length increases, the standard deviation for the radial acceleration decreases, and the effect of the pulsation absorption increases. Moreover, when the length is 330 mm, the percentage of the pulsation reduction is the largest, and the vibration suppression effect in the BHP is the best. This lays a certain experimental foundation for further optimization of BHPs.

6. Conclusions

In this paper, based on the vibration control in the double-layer BHP to the hydraulic pump port, the BHP with a three-layer structure is made by adding the SWCNTs. The simulation analysis and experiments are carried out, and the results are compared with those for the double-layer BHPs with RTV as the elastic layer, thus the following conclusions are obtained:

1. The RTV-SWCNTs composite is prepared by surface modification of the SWCNTs with noncovalent functionalization. And through the tensile test and SEM experiment, it is found that the CNTs are saturated in the composites when the content of the CNTs is 0.5 vol%~1 vol%, and the mechanical properties of the composites are better. When the content of the CNTs exceeds 1 vol%, the CNTs will agglomerate, which will reduce the mechanical properties of the composite. By comparing the experimental data, the mechanical properties of the RTV-SWCNTs composites are the best when the content of the CNTs is 0.5 vol%.
2. Based on the previously established BHP dynamic model, considering the influence of friction coupling, the dynamic model of BHP is modified. The response curve for the BHP in the frequency domain is obtained by solving the dynamic model with MATLAB software, and the modal test verified the correctness of the modified model.
3. The BHP with nanomaterials added is prepared, and the effect of the BHP on absorbing the flow pulsation and inhibiting pipeline vibration is verified through simulation analysis and experiments. Compared with the previous test data, the effect of the BHP with nanomaterials added on inhibiting pipeline system vibration is more obvious than that of the double-layer BHP with RTV as the elastic layer material. The effect increases with the increasing thickness of the elastic layer and increases with the growing length of the BHP.
4. This paper provides new theoretical and technical support for further design optimization of BHPs and the engineering application of vibration suppression.

In the following research work, we will conduct further research on the BHP. In this paper, only THF is used as a dispersant to disperse SWCNTs in RTV. We will explore better dispersion methods and matrix materials to improve the material properties in the BHP's elastic layer. The thickness and length of the BHP's elastic layer will be further optimized to find the optimum thickness and length for absorbing pipeline vibration and flow pulsation in the pump outlet pipeline.

Author Contributions: Conceptualization, C.G. and L.Q.; methodology, J.G.; software, J.G.; validation, J.G. and L.Q.; formal analysis, C.G.; investigation, J.G.; resources, L.Q.; data curation, J.Y.; writing—original draft preparation, J.G.; writing—review and editing, J.G.; visualization, J.Y.; supervision, C.G. and L.Q.; project administration, C.G. and L.Q.; funding acquisition, L.Q. All authors have read and agreed to the published version of the manuscript.

Funding: This research was funded by the National Natural Science Foundation of China, grant numbers (51775477 and 51505410).

Institutional Review Board Statement: Not applicable.

Informed Consent Statement: Not applicable.

Data Availability Statement: The data presented in this study are available on request from the corresponding author.

Acknowledgments: The authors gratefully acknowledge the financial support from the National Natural Science Foundation of China and the testing environment provided by Hebei Provincial Key Laboratory of Heavy Machinery Fluid Power Transmission and Control. The authors also thank China Scholarship Council for supporting the two-year research experience of Lingxiao Quan at the RWTH Aachen University and Washington State University.

Conflicts of Interest: The authors declare no conflict of interest.

Appendix A. Nomenclature and Numerical Values for the Parameters in the Theoretical and Simulation Models

Table A1. Structural parameters for the BHP.

Parameter Name	Value	Parameter Name	Value
Length of the pipeline (L)	0.33 m	The bulk modulus of stainless steel (K)	1.95 GPa
Inside diameter of the pipeline (r)	0.005 m	Young's modulus of stainless steel (E)	213 GPa
The thickness of the elastic layer (e_r)	0.005 m	Shear modulus of stainless steel (G)	81.9 GPa
The thickness of the stainless steel layer (e_t)	0.002 m	The density of elastic material (ρ_r)	1150 kg/m^3
Poisson's ratio for elastic material (v_r)	0.5	Stainless steel density (ρ_t)	7800 kg/m^3
Poisson's ratio for stainless steel (v_t)	0.3	Fluid viscosity (v)	10^{-5} m^2/s
Elastic material parameters C_{10}	−0.02593 MPa	Plug quality (m_t)	0.6 kg
Elastic material parameters C_{01}	1.733 MPa		

Appendix B. The Specification for the Experimental Apparatus and Measurement System

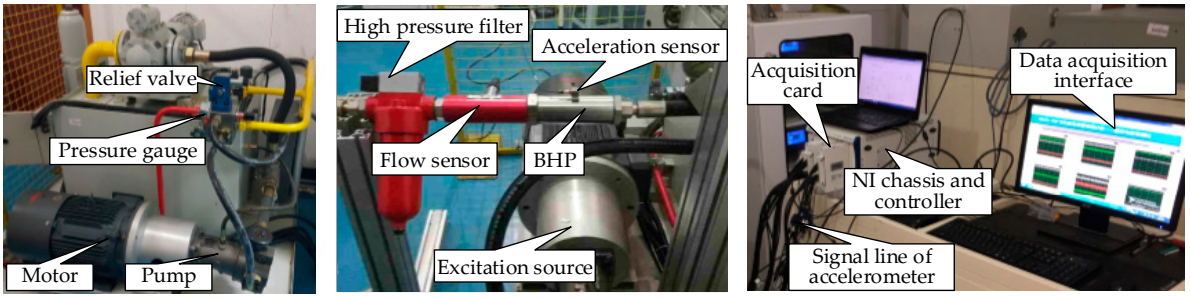

(**a**) (**b**) (**c**)

Figure A1. Installation of the vibration measurement pipeline system. (**a**) Hydraulic pump station; (**b**) installation of the BHP vibration measurement system; (**c**) measurement and control system.

Appendix C. Part of the Simulation Analysis and Experimental Data Results

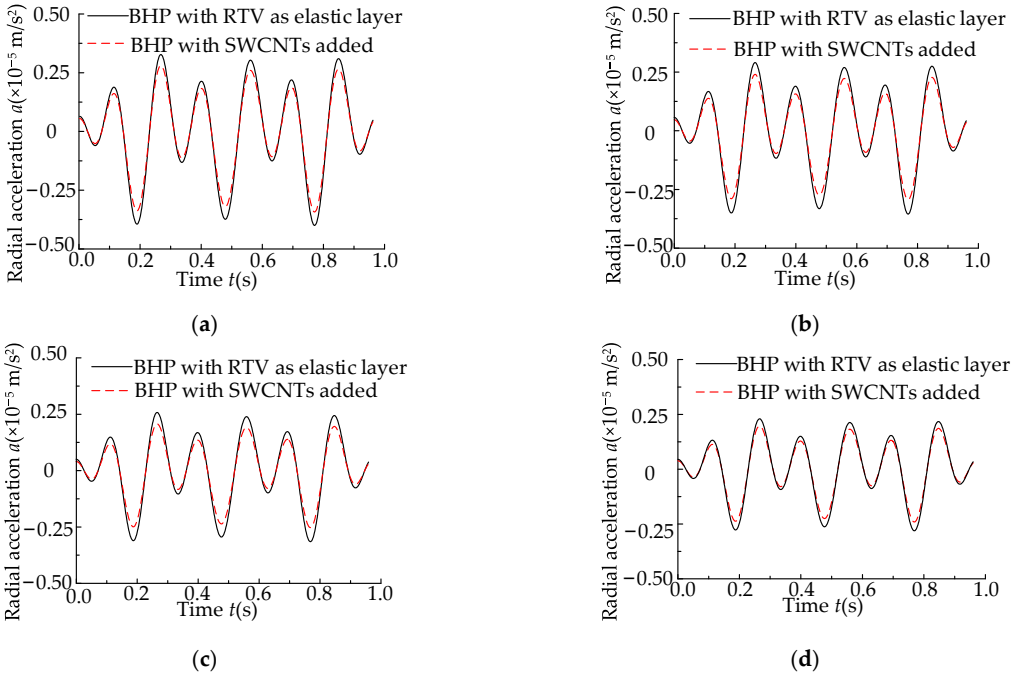

(**a**) (**b**)

(**c**) (**d**)

Figure A2. Radial acceleration at point P with different materials in the elastic layer. The length of the pipeline is: (**a**) 100 mm; (**b**) 150 mm; (**c**) 250 mm; (**d**) 300 mm.

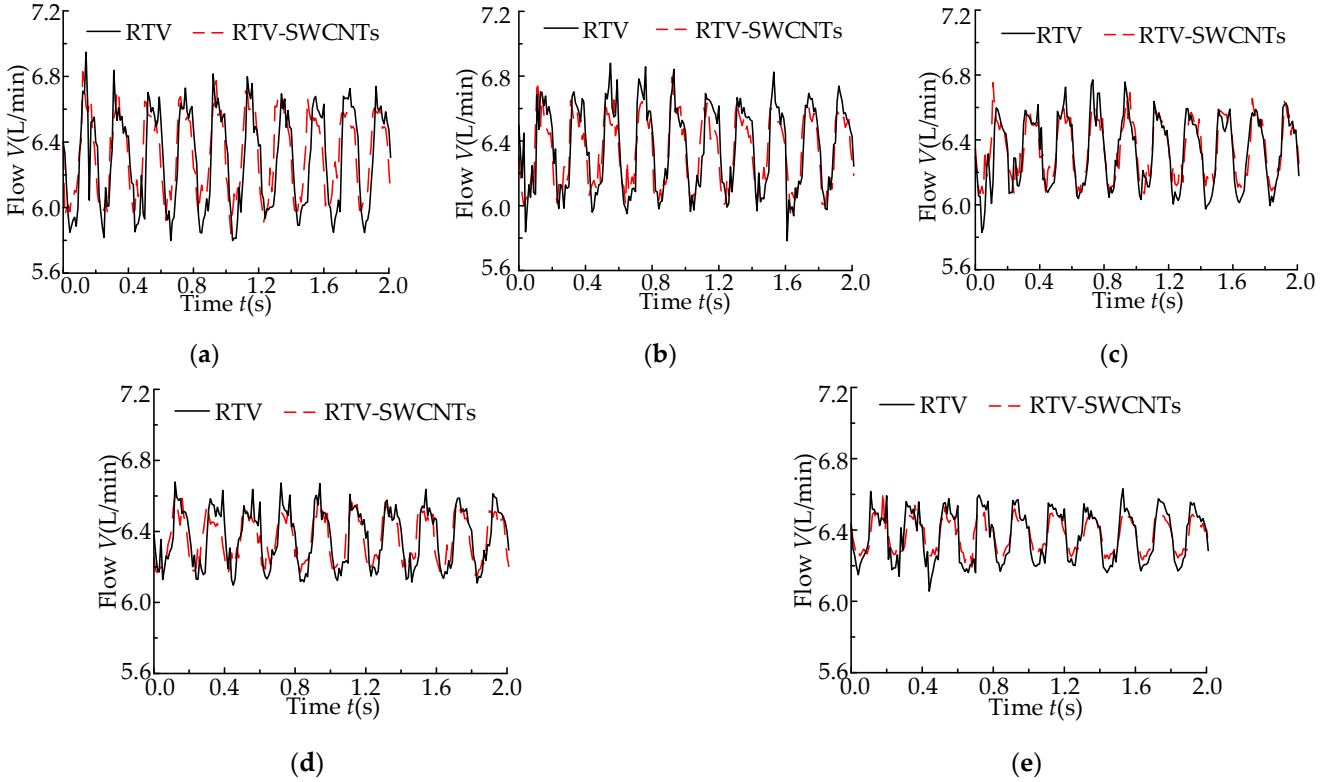

Figure A3. Effect of different materials on flow pulsation with the same length of the elastic layer. The length of pipeline is: (**a**) 130 mm; (**b**) 180 mm; (**c**) 230 mm; (**d**) 280 mm; (**e**) 330 mm.

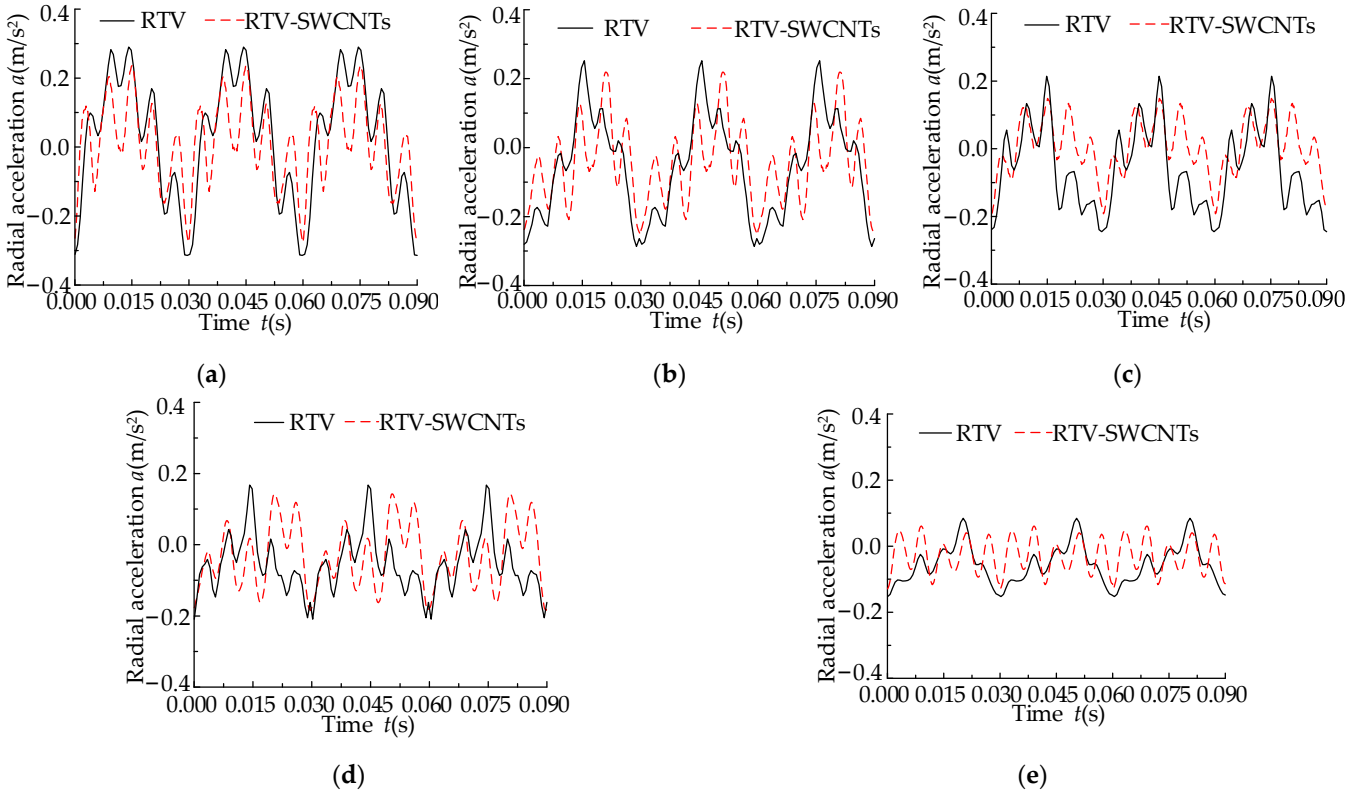

Figure A4. Influence of different materials on radial acceleration with the same thickness of the elastic layer. The thickness of the elastic layer is: (**a**) 5 mm; (**b**) 10 mm; (**c**) 15 mm; (**d**) 20 mm; (**e**) 25 mm.

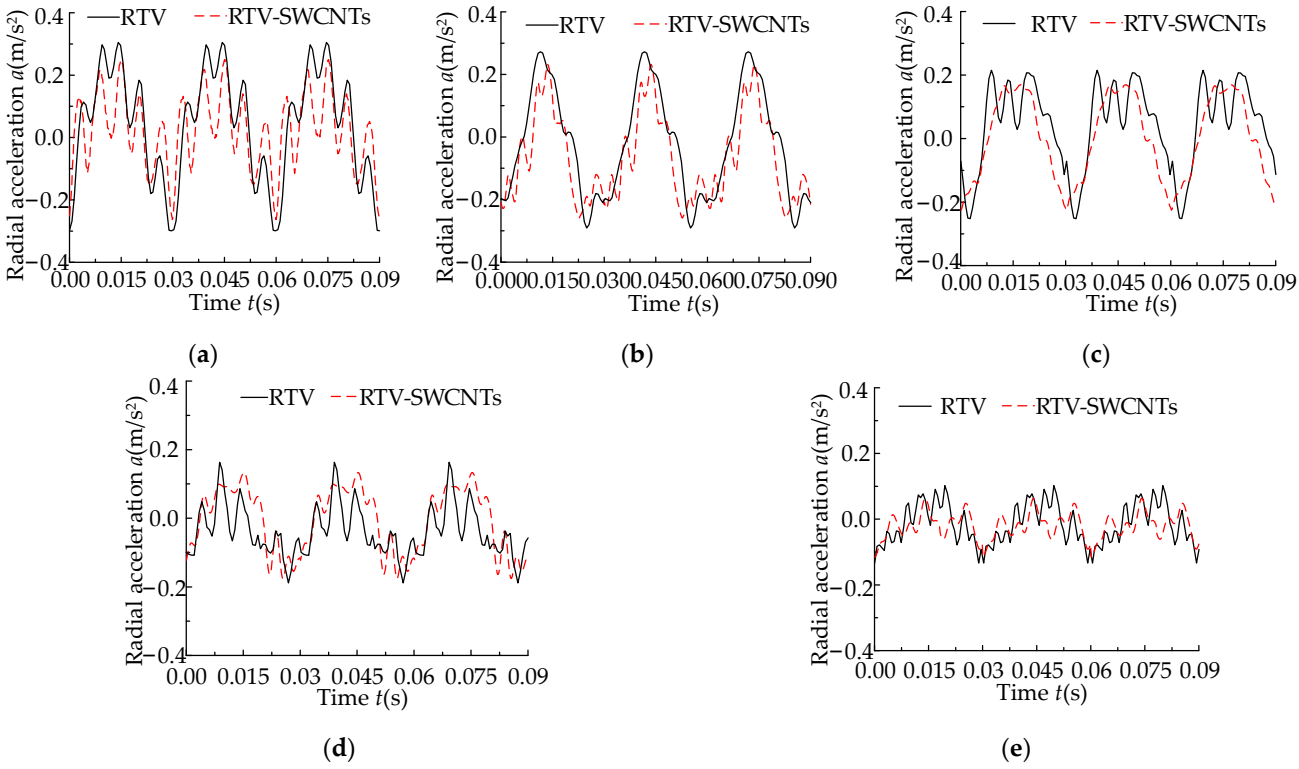

Figure A5. Effect of the elastic layer material on radial acceleration at the middle point in the pipe wall. The length of pipeline is: (**a**) 130 mm; (**b**) 180 mm; (**c**) 230 mm; (**d**) 280 mm; (**e**) 330 mm.

References

1. Zhang, L.P. *Hydraulic Transmission System and Design*; Chemical Industry Press: Beijing, China, 2005.
2. Wang, Z.L. *High-Pressure Hydraulic Energy System of Aircraft*; Beijing University of Aeronautics and Astronautics Press: Beijing, China, 2004.
3. Gao, F. Investigation into the Vibration Characteristic of the Pump and Connected Pipeline in the Aircraft Hydraulic System. Ph.D. Thesis, Zhejiang University, Hangzhou, China, April 2013.
4. Zang, J.; Xiao, R.H.; Zhang, Y.W.; Chen, L.Q. A Novel Way for Vibration Control of FGM Fluid-Conveying Pipes Via NiTiNOL-Steel Wire Rope. *Appl. Math. Mech. Engl. Ed.* **2023**, *44*, 877–896. [CrossRef]
5. Jiao, G.Y. Design of a Magnetic Interaction-Based Vibration Absorber for Continuous Beam. *Shock Vib.* **2020**, *2020*, 6384308. [CrossRef]
6. Chirathalattu, T.A.; Santhosh, B.; Bose, C.; Philip, R.; Balaram, B. Passive Suppression of Vortex-Induced Vibrations Using a Nonlinear Energy Sink—Numerical and Analytical Perspective. *Mech. Syst. Signal Process.* **2023**, *182*, 109556. [CrossRef]
7. Shu, C.L.; Yan, M.; Wang, C.; Sun, Y.; Du, F.; Chen, Q.D. Research on Typical Pipeline Design Method of Power Transmission Auxiliary System based on Vibration Control. In Proceedings of the 2022 8th International Forum on Manufacturing Technology and Engineering Materials (IFEMMT 2022), Chongqing, China, 14–16 October 2022. [CrossRef]
8. Shemshadi, M.; Karimi, M.; Veysi, F. A Simple Method to Design and Analyze Dynamic Vibration Absorber of Pipeline Structure Using Dimensional Analysis. *Shock Vib.* **2020**, *2020*, 2478371. [CrossRef]
9. Quan, L.X.; Zhang, Q.W.; Li, C.C.; Sheng, S.W. Sensitivity Analysis and Optimization for Support Parameter of Aviation Hydraulic Pipeline. *Chin. Hydraul. Pneum.* **2015**, *8*, 95–99.
10. Guan, C.B.; Jiao, Z.X.; He, S.Z. Theoretical Study of Flow Ripple for an Aviation Axial-Piston Pump with Damping Holes in the Valve Plate. *Chin. J. Aeronaut.* **2019**, *27*, 169–181. [CrossRef]
11. Cheer, J.; Daley, S. Broadband Active Control of Noise and Vibration in a Fluid-Filled Pipeline Using an Array of Non-Intrusive Structural Actuators. In Proceedings of the 44th International Congress on Noise Control Engineering, San Francisco, CA, USA, 8–11 August 2015. Available online: http://eprints.soton.ac.uk/id/eprint/380527 (accessed on 11 August 2015).
12. Zhang, Y.; Liu, X.; Rong, W.; Gao, P.; Yu, T.; Han, H.; Xu, L. Vibration and Damping Analysis of Pipeline System Based on Partially Piezoelectric Active Constrained Layer Damping Treatment. *Materials* **2021**, *14*, 1209. [CrossRef]
13. Zhang, Y.; Gao, P.; Liu, X.; Yu, T.; Huang, Z. Fluid-Induced Vibration of a Hydraulic Pipeline with Piezoelectric Active Constrained Layer-Damping Materials. *Coatings* **2021**, *11*, 757. [CrossRef]
14. Arenas, J.P.; Castano, J.L.; Troncoso, L.; Auad, M.L. Thermoplastic Polyurethane/Laponite Nanocomposite for Reducing Impact Sound in a Floating Floor. *Appl. Acoust.* **2019**, *155*, 401–406. [CrossRef]

15. Lubecki, M.; Stosiak, M.; Bocian, M.; Urbanowicz, K. Analysis of Selected Dynamic Properties of the Composite Hydraulic Microhose. *Eng. Fail. Anal.* **2021**, *125*, 105431. [CrossRef]
16. Mohammad, R.; Fred, N.; Labrosse, M.R. Processing, Manufacturing, and Characterization of Vibration Damping in Epoxy Composites Modified with Graphene Nanoplatelets. *Polym. Compos.* **2019**, *40*, 3914–3922. [CrossRef]
17. Swain, A.; Roy, T. Viscoelastic Modeling and vibration damping Characteristics of Hybrid CNTs-CFRP Composite Shell Structures. *Acta Mech.* **2018**, *229*, 1321–1352. [CrossRef]
18. Swain, A.; Roy, T. Viscoelastic Material Damping Characteristics of CNTs Based Functionally Graded Composite Shell Structures. *Proc. Inst. Mech. Eng. Part L-J. Mater. Des. Appl.* **2019**, *238*, 1510–1541. [CrossRef]
19. Pan, Y.; Liu, N.; Liu, A.; Chen, M.; Xu, W. Research on Microstructure and Mechanical Properties of Single-walled Carbon Nanotubes/7075 Composites. *Hot Work. Technol.* **2022**, *51*, 57–61. [CrossRef]
20. Quan, L.X.; Gao, J.; Guo, C.H.; Wu, S.D.; Yao, J.C. Dynamic Model and Response Analysis of Bionic Hydraulic Pipeline Based on Vascular Physiological Structure. *IEEE Access* **2019**, *7*, 67564–67575. [CrossRef]
21. Wang, J.W.; Zhang, J.; Fan, T.X. Processing Surface Treatment of Carbon Nanotubes and Its Applications to Copper Matrix Composites. *Mater. Rep.* **2018**, *32*, 2932–2939. [CrossRef]
22. Giambastiani, G.; Cicchi, S.; Giannasi, A.; Luconi, L.; Rossin, A.; Mercuri, F.; Fornasiero, P. Functionalization of Multiwalled Carbon Nanotubes with Cyclic Nitrones for Materials and Composites: Addressing the Role of CNT Sidewall Defects. *Chem. Mater.* **2011**, *23*, 1923–1938. [CrossRef]
23. Zydziak, N.; Hübner, C.; Bruns, M.; Barner, K.C. One-Step Functionalization of Single-Walled Carbon Nanotubes (SWCNTs) with Cyclopentadienyl-Capped Macromolecules via Diels-Alder Chemistry. *Macromolecules* **2011**, *44*, 3374–3380. [CrossRef]
24. Coleman, K.S.; Bailey, S.R.; Fogden, S.; Green, M.L.H. Functionalization of Single-Walled Carbon Nanotubes via the Bingel Reaction. *J. Am. Chem. Soc.* **2003**, *125*, 8722–8723. [CrossRef]
25. Huang, J.L.; Xie, G.J.; Liu, Z.W. Finite Element Analysis of Hyperelastic Rubber Materials Based on Mooney-Rivlin and Yeoh Models. *China Rubber Plast. Technol. Equip.* **2008**, *34*, 22–26. [CrossRef]
26. Freaktey, P.K.; Payne, A.R. *Theory and Practice of Engineering with Rubber*; Applied Science Publishers Ltd.: London, UK, 1978.
27. Wiggert, D.C.; Hatfield, F.J.; Stuckenbruck, S. Analysis of Liquid and Structural Transients in Piping by the Method of Characteristics. *J. Fluids Eng.* **1987**, *109*, 161–165. [CrossRef]
28. Zhang, Z.R.; Zhang, X.W. Numerical Manifold Method for Two Dimensional Steady Incompressible Viscous Flow N-S Equation. *Chin. J. Comput. Mech.* **2019**, *27*, 415–421.
29. Zielke, W. Frequency-Dependent Friction in Transient Pipe Flow. *Trans. ASME J. Basic Eng.* **1968**, *91*, 109–115. [CrossRef]
30. Brunone, B.; Golia, U.; Greco, M. Modeling of Fast Transients by Numerical Method. International Meeting on Hydraulic Transient and Water Column Separation. In *Proceedings of International Conference on Hydraulic Transients with Water Column Separation, Valencia, Spain, 4–6 September 1991*; Cabrera, E., Fanelli, M.A., Eds.; IAHR-Group: Madrid, Spain, 1991; pp. 273–280.
31. Vardy, A.E.; Brown, J.M.B. Transient Turbulent Friction in Smooth Pipe Flows. *J. Sound Vib.* **2003**, *259*, 1011–1036. [CrossRef]
32. Deng, B.C.; Li, J.S. *Rubber Plastic Blending Modification*; China Petrochemical Press: Beijing, China, 1996.
33. Yang, W.S.; Biamino, S.; Padovano, E.; Fuso, L.; Pavese, M.; Marchisio, S.; Vasquez, D.; Bolivar, C.V.; Fino, P.; Badini, C. Microstructure and mechanical properties of short carbon fibre/SiC multilayer composites prepared by tape casting. *Compos. Sci. Technol.* **2012**, 675–680. [CrossRef]